On the Mechanism of Electron Beam Radiation-Induced Modification of Poly(lactic Acid) for Applications in Biodegradable Food Packaging

Team PRODUCE: Chris Acha, Robert Blanchard, Jon Brodsky, Lilly Ding, Andrea Fox, Eleanor Grosvenor, Kalina Gibson, Annie Hoy, Justin Hughes, Kristen Lee, Olivia Mihok, Cade Stanfield, Ananya Uniyal, and Sydney Whitaker

Mentor: Mohamad Al-Sheikhly
Discussants: Luz Martínez-Miranda, Lawrence Sita, Tao Lowe, Qin Wang

Thesis submitted in partial fulfillment of the requirements of the Gemstone Honors Program, University of Maryland, 2022

Abstract

Poly(lactic acid) (PLA) is a biodegradable polymer used for food packaging. The effects of electron beam radiation on the chemical and physical properties of amorphous PLA were studied. In this study, amorphous, racemic PLA was irradiated at doses of 5, 10, 15, and 20 kGy in the absence of oxygen. Utilizing electron paramagnetic resonance spectrometry, it was found that alkoxyl radicals are initially formed as a result of C-O-C bond scissions on the backbone of the PLA. The dominant radiation mechanism was determined to be H-abstraction by alkoxyl radicals to form C-centered radicals. The C-centered radicals undergo a subsequent peroxidation reaction with oxygen. The gel permeation chromatography (GPC) results indicate reduction in polymer molecular mass. The differential scanning calorimetry and X-ray diffraction results showed a subtle increase in crystallinity of the irradiated PLA. Water vapor transmission rates were unaffected by irradiation. Further mechanical testing showed mechanical properties in line with reduced molecular mass. In conclusion, these results support that irradiated PLA is a suitable material for applications in irradiation of food packaging, including food sterilization and biodegradation.

Acknowledgements

We would like to thank our mentor, Dr. Mohamad Al-Sheikhly, for providing us with support and guidance throughout the past four years; Lorelis González López, Catherine Lewis, Dr. Kim Morehouse, Steven Guerin, Zois Tsinas, Aiysha Ashfaq, and Eli Fastow for training us in lab skills and protocol; Dr. Lawrence Sita, Charlotte Wentz, Dr. Stas Stoliarov, Jacques De Beer, Dr. You Zhou, Dr. Peter Kofinas, Kyle Ludwig, and Rebecca Fedderwitz for their generosity in allowing us to use their lab equipment; Dr. Fred Bateman and the Dosimetry Group within the Radiation Physics Division at the National Institute of Standards and Technology; our librarians, Ms. Stephanie Ritchie and Ms. Marcella Stranieri, for helping us conduct our literature review and propose our research; and the Gemstone staff and faculty— Dr. Kristan Skendall, Dr. David Lovell, Dr. Leah Tobin, Dr. Vickie Hill, Jalah Townsend, and Jessica Lee— for supporting our research endeavors. We would also like to acknowledge the Maryland Sea Grant, National Oceanic and Atmospheric Administration, U.S. Department of Commerce for funding this project through the awards NA14OAR4170090 and NA18OAR4170070.

Chapter 1

1.1 Overview of Research Problem, Purpose, and Rationale

Introduction to Food Waste

Food waste is a substantial concern worldwide, as a significant portion of all farmed produce spoils before consumption [1]. It is estimated that around 1.3 billion tons, or around a third of all food produced for humans, is wasted per year, including 45% of all fruits and vegetables [1]. Many steps during production and the supply chain process contribute to food waste. Spoilage is a major type of loss that occurs in each step of the production process [2]. Food can be exposed to insects, rodents, bacteria, and other harmful environments that contribute to expedited spoilage [3]. Spoilage can also occur due to equipment malfunction at the retail level and when consumers buy more food than they can eat [4].

When spoiled food is thrown away, it often ends up in a municipal waste landfill where it produces harmful gasses like methane and carbon dioxide during decomposition [2]. Additionally, the more food that is thrown away, the more resources required for food production such as water, fertilizers, and space are wasted [5]. The nitrogen fertilizers used by farmers can degrade nearby water sources, causing contamination and algal blooms [5].

The United Nations' 2030 Global Goals for Sustainable Development include both *Responsible Consumption and Production* and *Zero Hunger* [6]. Their aims are to "end hunger, achieve food security and improved nutrition and promote sustainable agriculture" and to "halve per capita global food waste" by minimizing the amount of food lost at every phase of production, including harvest, retail, and after the food has reached consumers [6]. In theory, global food production can provide for every living person, indicating that food spoilage and

ineffective distribution of food are substantial contributors to world hunger. These are problems that can be improved with new technologies and improved distribution practices [7].

Ramifications of Food Spoilage

In our current food distribution system, industrialized agriculture has created monopolies in the food production industry [8]. Consequently, produce in the United States must undergo long periods of storage as it travels thousands of miles across the country before reaching its final destination [8]. To accommodate this business model, farmers make sacrifices concerning the quality of their produce. Growing crops are covered with chemical fertilizers and pesticides to increase yield, and ethylene gas is sprayed on harvested produce to prevent it from ripening naturally, thereby increasing shelf life [8]. However, a great deal of produce still ripens prematurely and becomes inedible before even reaching consumers [9].

Areas most affected by ineffective food distribution are known as food deserts [10]. Food deserts are geographic areas where residents have few to no convenient options for securing affordable and healthy foods — especially fresh fruits and vegetables [10]. Disproportionately found in high-poverty areas, food deserts create extra, everyday hurdles that can make it harder for children, families and communities to access fresh foods [10]. Generally, food deserts are most commonly found in areas with smaller populations, higher rates of abandoned or vacant homes, and residents who have lower levels of education, lower incomes, and higher rates of unemployment [11]. It was found that as neighborhood poverty increased, supermarket availability decreased [11]. Food deserts are a disproportionate reality for Black communities, and at equal levels of poverty, Black census tracts had the fewest supermarkets [11]. Ineffective

food distribution systems are a driving force behind food deserts and solutions to food distribution, spoilage, and waste are necessary to eliminate them or reduce their impact.

Packaging Solutions

A 2012 study asked participating families to evaluate their levels of food waste, including what types of food they wasted and for what reasons they were wasted. The results of this study concluded that 20-25% of the families' food waste in 2012 could be attributed to packaging [12]. Currently, most discarded packaging products are sent to landfills [13] and in 2009, packaging waste accounted for 29.5% of the municipal solid waste in the United States [13]. Although some plastics are biodegradable in nature, many do not degrade in landfills [14]. In general, degradation occurs for most biopolymers when in contact with water, and many are only degradable at industrial composting facilities [14], [15].

To combat this issue, many grocery stores and food distributors are in the process of diverging from single-use plastic packaging. For example, Trader Joe's has made a commitment to remove many single-use plastics from its stores, mostly from the produce department [16]. With an ever growing global population that relies on fresh food, innovative plastic solutions for food packaging have become increasingly necessary.

There is much potential for innovation and research that aims to combine both environmentally-friendly and consumer-friendly materials with packaging designs that increase the shelf life of produce. The implications for future research in this field include decreasing food waste at various phases of the food delivery process, as well as decreasing the use of disposable plastics and harmful packaging materials. Successful research in this area can

increase sustainable practices in a variety of industries, and will ultimately create a positive, long-term environmental impact and decrease food insecurity.

The modification of standard food packaging will provide a comprehensive solution to these problems. Enhancing food packaging can improve food quality while also keeping food fresh longer and allowing more time for shipping. Modifications to packaging will include making the material more biodegradable than current standards, which can help counteract waste created by plastic in landfills [17].

The research in this paper focuses on modifying the biopolymer, poly (lactic acid) (PLA). PLA is a non-toxic, compostable bio-based material derived from starch and/or sugar [18]. The Food and Drug Administration classifies PLA as GRAS (Generally Recognized as Safe) for use in food and beverage packaging [19]. PLA is also able to maintain a carbon-rich environment which decreases microbe growth and maintains a low pH, delaying the spoilage of food [20].

Ionizing radiation creates free radicals that can react through crosslinking or chain scission. Crosslinks are covalent bonds between separate polymer chains, formed when two C-centered radicals combine. Chain scission occurs when these C-centered radicals react with oxygen in the atmosphere. The balance between crosslinking and chain scission is affected by dose and environment [21]. Our original goals of the project were to enhance crosslinking in order to create a denser polymer network that would prevent gas from diffusing through the membrane.

1.2 Method Framework and General Research Questions

In this investigation, we use multiple quantitative research methods to make conclusions about the viability of our packaging material. Primarily, we use experimental research to collect and analyze data. We planned to supplement this work with computational modeling to compare

our findings with existing literature, but this ongoing research has not yet produced results. We further explain this approach in Section 1.3. We originally planned to include a survey to better understand the position of our local community on biodegradable food packaging, which we would use to evaluate the success of our material. Ultimately, we decided instead to target government regulations that have control over the commercial production of the material. We believed that consumers' opinions would be more important in future iterations of the material design, and that we must first target FDA approval.

The main goal of this research is to modify biopolymers to create a biodegradable food packaging that aims to reduce food and plastic waste by discouraging food spoilage. The aim of our research was to answer the overarching question: How can we modify polylactic acid, a biodegradable polymer, for applications in food packaging to extend the shelf life of produce?

With each stage and aspect of the project, the research aimed to examine some more detailed questions, which included:

1. What is the impact of electron beam irradiation on the structure of polylactic acid? Is crosslinking or chain scission more common? What are the predominant reactions?
2. How can we modify the polymer structure to have selective permeability of oxygen, carbon dioxide, and water vapor?
3. How will different electron beam irradiation doses impact the thermal and mechanical properties of the polymer? What are reasonable characteristics for food packaging?
4. How can computational studies using Monte Carlo simulations and COMSOL corroborate experimental results? What added information do they provide?

5. How can we ensure that the modification process is environmentally friendly and possible on a large scale? How can irradiation be used in degrading the polymer after its use?

1.3 Significance of Findings and Limitations

Our findings led us to win an award at the Do Good Showcase in Fall 2020, where we discussed the impacts of reducing both food and plastic waste, in line with the United Nations' Global Goals for Sustainable Development. We also presented at the UMD Undergraduate Research Day in Spring 2021. Most notably, we published a peer-reviewed article in the journal *Applied Sciences* in Spring 2022.

There were several limitations which slowed our progress significantly, most notably the COVID-19 pandemic. Initially we had hoped to have all of our members conduct laboratory research, however we were instead limited to six students. In addition, we lost much of our Spring 2020 semester due to entirely virtually schooling. We had initially planned on testing PLA and then moving on to a promising blend of PLA and poly(hydroxybutyrate) (PHB) and PLA that we processed ourselves with TAIC, an additive known to encourage crosslinking during irradiation. However, due to time and man-power constraints, we were forced to remain with our initial samples. These original samples were obtained from ExTech plastic and theorized to be neat, commercial grade PLA, with our initial FTIR confirming this to a high degree of certainty. Due to lack of data sheets and response from the vendor, we were never able to obtain company records as to the content of our PLA. We were able to characterize the PLA using DSC, FTIR, and optical microscopy, eventually. This revealed that our PLA was in fact a racemic copolymer of neat PL(D,L)A with negligible crystallinity.

The original scope of our paper was focused on the formation of crosslinks in PLA to improve it for food packaging applications. However, this crosslinking is greatly enhanced by additives such TAIC, which are found in nearly all commercial grades of PLA. Without additives the expected dominant effect of irradiation would be chain scission rather than crosslinking. The need to stick to these samples forced us to pivot our research to a more academic review of irradiation of our specific polymer, rather than a project focused on creating a food packaging deliverable.

Another limitation came from the usage of our in-lab DSC. We had originally planned on using that equipment without charge, but instead had to pay to use another lab's DSC. As our DSC was improperly tuned to detect the more subtle changes in heat flow due polymer phase transitions. The combination of time lost attempting to calibrate our DSC and limits imposed by budget, limited the number of samples we could run of DSC, notably preventing us from characterizing the thermal properties of 10 and 50 kGy samples. Budgetary limitations prevented us following up on interesting trends in the data that could have been further analyzed. For example, our double melting peak could have been analyzed at multiple ramp speeds to better determine if it were due to stereocomplexation, crystallite size, or multiple crystalline phases. Our current theory is that our double melting peaks are caused by a transition from imperfected to perfected spherulites; a theory which is supported by our data and reaction mechanisms. However, the sensitivity of this transition to heating rates would allow us to obtain a more definitive answer.

The limitations on man power had an effect on our ability to characterize our irradiated PLA. Since fewer people were allowed in the lab, we were not able to run as many permeability tests as anticipated. In addition, there were issues ordering materials and designing a testing

apparatus, which limited our ability to test CO_2 and O_2 permeability. The standard methods for testing these gas permeabilities required more resources and set-up as compared to water vapor. Due to the fact only a small portion of the team was allowed in the lab, we were unable to test these properties as we would have liked.

The COVID-19 pandemic also limited the number of times we were able to irradiate our PLA samples, since the laboratories at NIST were running at limited capacity and limited to outside users. This is another reason we were forced to focus our efforts on our neat PLA. As previously mentioned, we were unable to irradiate any PLA with additives limiting our ability to evaluate irradiated PLA as a plausible sustainably packaging material. Commercial PLA will contain both plasticizers and additives, so neat PLA will not reflect the effects of irradiation as accurately.

Chapter 2

2.1 Microbiology

In food packaging applications, it is important to consider the ability of the package to keep out spoilage organisms, including yeasts, molds and *pseudomonas* bacteria [22]. Another important consideration is the ability of the packaging to regulate the atmosphere to keep the contents fresh for longer [23]. Some factors influencing spoilage include oxygen, carbon dioxide and nitrogen gasses [24]. Oxygen promotes anaerobic growth and oxidative rancidity [25]. Carbon dioxide modifies the intracellular pH and fosters the growth of *Lactobacillus, Carnobacterium, Brochothrix and Enterococcus* bacteria [26]. Preparation can influence spoilage because if the food is comminuted, where it has been chopped or grinded and restructured, there will be a higher initial microbial load due to the use of a lower quality product for grinding [27].

Several species of bacteria occur more often on comminuted food than intact foods [27]. Cooked food can be contaminated by bacteria that survive heat processing [27]. Vegetables are generally capable of supporting growth of bacteria, yeasts and molds as they have a pH of 4.5-7.0 and a water activity of 0.98 [27]. Any bruising, punctures, cracks and cuts can result in loss of integrity and enzyme-facilitated damage that fosters microbial growth [27]. Overall, a quality packaging material must protect the item from spoilage by maintaining low levels of oxygen and water vapor [23].

2.2 Irradiation of Commercial Food Packaging

Irradiation is performed on less than one tenth of one percent of fruit, vegetables and meats imported by the US [28]. Irradiation is done for many reasons including prevention of foodborne illness, preservation, control of insects, delay of sprouting and ripening and sterilization [28], [29]. Irradiation can effectively eliminate organisms that can cause foodborne illness including *Salmonella* and *Escherichia Coli* [28]. Preservation can be completed with irradiation to extend the shelf life of foods by destroying or inactivating organisms that cause decomposition [28]. Control of insects is an essential part of irradiating imported foods because insects that come into the US from other countries can be invasive to our native species [28]. Irradiation also reduces the need for other pest controlling methods such as pesticides, which increase the risk of certain health issues in humans and damage to crops [28]. Irradiation can also be used to inhibit sprouting on root vegetables such as potatoes, and ripening of soft produce such as fruits [28]. Sprouting can lead consumers to avoid purchasing the vegetables, as they now view it as overripe or rotten. The quick ripening of fruits can become an issue when there is not enough time for transport, storage and sale before the product becomes overripe. Reducing

the speed at which the produce respires through irradiation can reduce the overall ripening speed, increasing the likelihood that the product will sell before becoming too ripe [28]. Sterilization is the last reason that food is irradiated in the US. This reason is the focus of our research study. This process allows foods to be stored for months or even years without refrigeration. These foods are important for people with compromised immune systems, as any pathogenic bacteria can become extremely dangerous [28].

All irradiated food packaging in the USA must first be approved by the FDA before commercial use. There are two main methods for new materials to be approved, a Food Contact Notification (FCN) or via the Threshold of Regulation (TOR) [30]. FCN are used when new Food Contact Substances are in need of approval. FCN are required to have a comprehensive summary of the substance, a detailed chemical identity, the intended conditions of use of the substance, the intended technical effect, an estimation of intake, and a toxicity and environmental impact report [31]. The summary should include discussion of the information in the rest of the report, including dietary exposure, potential impurities, toxicity report, and any other safety data included in the FCN [31]. An in-depth toxicity report is required, which identifies adverse effects of the substance. Toxicity tests are performed generally and additionally *in vivo* [32]. The toxicity report must include a risk assessment for carcinogenic constituents of the original substance. Finally, a report must include an environmental assessment of the substance. After a FCN is submitted, the FDA has 120 days to reject the FCN, otherwise the FCN is approved [33].

The other method of approval is via TOR, which are limited to substances used in food packaging which do not have a technical effect on the food [34]. Requests should contain the following information: the chemical composition of the substance in accordance with CAS (Chemical Abstract Service), the intended technical use of the substance, information on the

conditions of use, a "statement as to whether the request for exemption from regulation as a food additive is based on the fact that the use of the substance in the food-contact article results in a dietary concentration at or below 0.5 ppb, or on the fact that it involves the use of a regulated direct food additive for which the dietary exposure is at or below 1 percent of the acceptable dietary intake," information allowing the daily dietary consumption of the substance, a literature based toxicological report, and a claim of categorical exclusion or an environmental assessment [34].

2.3 Current Problems in Food Production and Business

Transforming current food systems and packing methods for affordable, healthy diets are a key driver to assist with the current state of food security and nutrition in the world. Given the current COVID-19 pandemic that continues to evolve, it will be foreseen that there will be impacts on the current state of food security and nutrition in many countries [35]. It is important to recognize the influence that biodegradable, irradiated food packaging can have on the shelf life of produce for consumers.

The current supply chain in which food is distributed has a large impact on the availability of fresh produce for consumers. The value chain, in which food travels from production to consumption, includes handling and storage, processing and packaging, and distribution to markets [36]. It has been noted that emerging economies waste 40% of food during the production and storage steps of the value chain [37]. Our packaging seeks to allow food to withstand long storage times through the irradiation of produce packaging. Due to poor storage facilities and transportation infrastructure, oftentimes food is unable to reach the last steps of the value chain, and rendered as non-consumable by consumers [38]. In contrast, mature

economies who have storage facilities and transportation infrastructure often reach issues in the later steps of the value chain, including overconsumption by consumers and the inability for food to withstand long periods of storage once in the hands of grocery retailers or consumers [37]. This leads to stores throwing away food and an increased amount of food waste every year.

Similarly, the US Department of Agriculture indicates several key factors influencing the wastage of food in developed countries. Among them, aesthetic standards and consumer preferences for produce at any step of the supply chain heavily impacts food that is thrown away [39]. The demand for buyers who might not accept a seller's produce if it is not aesthetically up to their standards, and this leads to produce being thrown away [39]. In addition, the culture of agribusiness involves a group of large companies, or an oligopoly, which primarily deal with the agricultural produce and services required in farming. As mentioned in Chapter 1, due to the nature and structure of these companies and their domination of the produce market, this creates monopolies and subsequently long periods of storage for food traveling across the country. In finding ways to limit the decay of food, packaging has become one of the key factors that can be targeted to mitigate food loss during those long periods of storage.

Current solutions are not catch-all or inclusive of all of the needs of consumers. Solutions such as using crop varieties of a lower nutritional value allow food to remain ripe for a longer period of time post-harvest, and similarly covering growing crops with chemical fertilizers increases the yield of food. However, both solutions only lead to more food waste throughout the process, as buyers still deem the food unsatisfactory. Price volatility of produce, such as during times of higher prices, leads to more harvesting, poor worker treatment and lower quality food and increased loss further along the supply chain [40]. In addition, recent consumer trends have shown a preference for organic, non-pesticide produce to contribute to a healthier lifestyle [40].

A statement by McKinsey and Company reveals the pandemic's influence on consumer preferences [41]. The COVID-19 pandemic caused an increase in price consciousness of consumers as well as more of a focus on hygiene and health. Thus, the food system should be viewed as an integrated whole. Strategies and public policy initiatives should be developed to comprehensively address the entire integrated system. Coordinating both the vertical and horizontal participants within the food chain through agribusiness economics is essentially the goal of biodegradable packaging that extends shelf life.

2.4 Packaging Solutions

There have been various ventures into the realm of packaging solutions to address food spoilage issues. One such endeavor is active packaging, where the environment is actively adjusted to be optimal. There are two types of active packaging: active-scavenging and active-releasing systems [42]. Active-scavenging systems typically target moisture, carbon dioxide, oxygen, and ethylene, which all lead to food spoilage. One common example is oxygen scavengers, most commonly the iron-based scavenger, where the reduced iron is irreversibly oxidized [42]. Ethylene, a plant-growth hormone that induces ripening, can be scavenged using substances such as potassium permanganate [42]. Examples of active releasing systems include antioxidant releasers, carbon dioxide emitters, and antimicrobial packaging.

Modified atmosphere packaging (MAP) is another type of active packaging that replaces atmospheric air with a mix of gasses, primarily carbon dioxide, preserving food and limiting oxygen exposure [43]. Our original planned design is a variation of MAP. Carbon dioxide delays food spoilage by maintaining a low pH and thus decreasing microbial growth. Other compounds such as N_2 and O_2 are needed in small amounts to prevent package collapse or for desired food

outcomes. This packaging method is particularly useful for meat, fish, dairy, and poultry products, which tend to have a short shelf life especially in the presence of oxygen.

In smart packaging, chemicals emitted during the produce ripening process react with packaging sensors to produce a color change when the food is ripe. Changes in pH detected by these sensors could indicate bacterial growth, whereas different sensors are able to detect changes in the amine levels of meat, poultry, and fish [44]. Although smart packaging is a revolutionary idea in theory, with present technology, it is expensive to design and produce these sensors, making them less feasible as a universal solution currently.

2.5 Materials Selection Considerations

When consumers go to the grocery store, the visibility of produce is a crucial component of being able to assess its quality. Therefore many optical properties of packaging films, such as color, transparency, and gloss, can greatly impact consumer opinions of the product [45]. In a 2014 study, more than half of individuals who completed the survey believed that in general, food should be contained within transparent packaging, regardless of whether it was fresh produce or other products [46]. Transparent packaging is preferred because the consumer is more easily able to examine the product, and therefore more likely to trust the freshness and quality [46].

Color changes should be a consideration when using additives in bioplastic packaging. For example, when coriander and tarragon essential oils are added to the films, they have a yellow hue, whereas grape seed extract films have a brown color [45]. When different additives are incorporated into the film, the opaque index increases, meaning that the film becomes progressively less and less transparent. In addition, the opacity has been predicted to be related to the film thickness [45]. These are two factors that will be very important to consider when

choosing a biopolymer and additives, given that the transparency of the packaging does have such a large role in consumer attitudes towards buying produce [46].

Similar to transparency, the texture of food packaging can have an impact on the consumers' perception of the food. In one study, the researchers had the participants hold the packaging in their non-dominant hand, while eating the manufactured food with their dominant hand [47]. The main objective was to observe if the texture of the packaging impacted the participants' views on the texture and other characteristics of the food [47]. One experiment concluded that when food and its packaging had similar textures, the texture of the packaging affected consumers' perception of the contents' texture. When consumers held biscuits in a pot with a rougher texture, they rated the biscuits as being crunchier and harder [47]. This study demonstrates the impact of the parallels between package texture and food texture perception. As food texture is known to have an impact on the perception of food quality and freshness, it is important to be mindful of how closely the packaging texture mimics that of the food being packaged.

The mechanical properties of the film are also important to consider when choosing a biopolymer. Tensile strength, elastic modulus, and elongation at break are all values that relate the mechanical properties of the polymer film to the chemical structure [48]. Packaging films must be strong enough to withstand harsh conditions during manufacturing and shipping, so the proper polymer must be used for the greatest effectiveness. In general, adding essential oils or extracts to a film causes a decrease in tensile strength and an increase in the elongation at break [49]. In contrast, when researchers have added nanoparticles to the films, the tensile strength increased because the nanoparticles reinforced the chemical structure of the polymers [48].

Flexibility is an important property for plastics in practical use. If the plastic in question

is not flexible enough, the deformation remaining can alter the effectiveness of the plastic for its intended use. Depending on the conditions of the plastics, the appropriate amount of plasticizers can be determined, which when added to a plastic, can alter its flexibility. As mentioned earlier, a problem with plasticizers is that they can leach out of the plastic over time and into food, but also cause the plastic to lose the flexibility gained by the plasticizer [50].

Water vapor permeability (WVP) identifies the amount of water that is able to pass through the polymer membrane. WVP is important to consider while dealing with food packaging because water can be a catalyst in food degradation, so restricting water flow into the package is of the utmost importance [51]. In general, WVP decreases when additives are added to the polymer films, and as the concentration of additives increases, the WVP continues to decrease [51]. This occurs because there is less free space in the intermolecular matrix, so water has a more difficult path for permeation [48]. Another method to decrease water vapor permeability is to increase crosslinking, which creates tightly knit connections within the three-dimensional arrangement, decreasing space for water molecules [52]. Currently, finding an appropriate bio-based polymer to use can be rather challenging because they are typically hydrophilic in nature, allowing for the passage of water molecules through the material [52].

Film solubility is extremely important when developing food packaging. Packaging polymers should usually be insoluble and hydrophobic with high water resistance and long shelf life [53]. Adding plasticizers to polymer films can increase solubility because they decrease the bond strength between polymers, which provide space for water molecules to enter [53]. Solubility in water, or lack thereof, is important in evaluating the practical applications of the biopolymer options. Hydrophilic materials prefer interactions with water as compared to nonpolar substances, such as oil. The hydroxyl group on the polymer is responsible for the

majority of its hydrophilic properties, and this issue can be combated by substituting with a hydrophobic ester group [52]. Similar to WVP, this is an important factor to consider when choosing a biopolymer because water promotes the oxidative process of food.

Gas barrier properties of the biopolymer film are another concern, particularly for oxygen and carbon dioxide. When in contact with oxygen, fresh produce is likely to spoil faster because oxygen, like water, increases the rate of oxidation. Most biopolymers have reasonable barrier properties in low levels of oxygen concentration, but begin to falter in an abundance of oxygen [52]. The biopolymer must have a certain threshold for oxygen permeability so that the food has a reasonable shelf life that satisfies consumers' requirements [54]. In some situations, lack of resistance to oxygen can cause the biopolymers to degrade, reducing their effectiveness as a packaging material [54].

Thermal properties are another important consideration. From production to waste, packaging is exposed to thermal stress. Thermodynamic properties can be evaluated under different conditions, such as heating and cooling at different atmospheric pressures [52]. Greater crosslinking has been cited as a way to improve the thermal properties of a biopolymer film due to the increase of strong, covalent bonds within the film [52]. One value that can be used to quantify thermal stability is glass transition temperature, which refers to the temperature below which the plastic structure changes from primarily amorphous to crystalline. This also marks the change of the plastic going from being soft to hard and brittle [50]. The glass transition temperature should preferably be low, so that the polymer will not change its properties during usage. Simultaneously, the melting point should be high so that the plastics do not melt during use. Different polymers react differently to exposure to heat; some are thermoplastics, while others are thermosets [50]. Thermoplastics melt when exposed to heat and harden when cooled,

whereas thermosets experience crosslinking and subsequent degradation [50]. The highest temperature at which a polymer can be used is restricted by the temperature at which degradation begins and its use is no longer feasible [50]. Additives and thermo-stabilizers can be inserted to alter a film's thermal properties. In relation to traditional types of plastics, it is important that we increase the thermal stability of the biopolymers to make their resistance to heat comparable to our target industry standards.

Although most biopolymers are safe for human exposure, it is important to consider the toxicity of compounds and processes used. If food packaging is not deemed safe for humans, then placing it in such close proximity to food presents the possibility that the toxicity can leach into the food [15]. Natural crosslinking agents are safe and effective in strong bonds in biopolymers, whereas synthetic crosslinking agents have quite adverse effects [15]. These include carbodiimide and hexamethylene diisocyanate, which are both cytotoxic and evoke harmful responses from the body [15]. In addition, some additives, specifically silver nanoparticles, can be toxic to the human body, causing inflammation among dermal and pulmonary cells. When exposed through food packaging, it is also possible that the nanoparticles can migrate into cells, leading to internal organ damage [55].

Antimicrobial properties aid in biopolymer resistance to microorganisms, such as fungi and bacteria, that commonly accelerate the food degradation process. Currently, the main cause of food spoilage is microbial contamination. If the chosen polymer does not have intrinsic antibacterial properties, we can incorporate certain groups of additives that are antimicrobial agents, including: metal ions, essential oils, plant extracts, polysaccharides, peptides, and enzymes, in addition to synthetically-produced agents [56].

Although all of these considerations are important when deciding between different

biopolymers for plastics, the most important is biodegradability. Our main goal with this research is to combat the issue of single-use plastic, so it is imperative that our plastic can break down naturally within a short enough period of time. Sources for biodegradable plastics are common since they are abundant in nature and can be derived from waste [57].

2.6 Biodegradable Polymers for Consideration

Chitin is a macromolecule that can be extracted from the shells of crustaceans [57], [58]. Chitin can be degraded by chitinase and its fibers can be used in biomedical devices. Chitin has been used as a drug carrier, artificial skin, and sutures where it provokes a similar reaction to PGA. Although it is not water soluble, its partially deacetylated form, chitosan, is soluble [57], [58] and has been used for cosmetics and wound treatment [58]. Chitosan can be processed to have similar mechanical properties as synthetic PE film, as well as being able to block ultraviolet light [59]. In addition, chitosan can have an antimicrobial effect against fungi, yeast, and bacteria due to protonated amino groups dissolved in acid, or potentially the hydrolysis products on microbial DNA [57], [60]. Chitosan can be crosslinked for superior physical, mechanical, and potentially, thermal properties [52], [57]. However, chitosan degrades before its melting point, meaning that it cannot be molded, extruded, or heat sealed without being blended with thermoplastic polymers [57]. In addition it has high water vapor permeability, requiring modifications of deacetylation degree, pH, solvent type or plasticizers, polymer blending, or crosslinking [57]. Blending PLA with chitosan is commonly used in the biomedical industry for use as a chelating agent, drug carrier, membrane, water treatment additive, biodegradable pressure-sensitive adhesive tape, wound healing agent,and nerve repair agent [61]. A hydrogel could be synthesized by grafting lactic acid onto the amino groups of chitosan [61].

Poly(lactic acid) (PLA) is an alternative to petroleum-based plastic packaging that is derived from renewable resources [62]. It is one of the most researched and currently used biodegradable aliphatic polyesters [63]. PLA is recognized for its biodegradability, transparency, and film-forming properties, however, its disadvantages include low degradation rate and brittle breakage [61]. It has mechanical and barrier properties comparable to poly(styrene) (PS) and poly(ethylene terephthalate) (PET), and is commercially produced with a low production cost [62], [63]. To enhance the mechanical and biological properties of PLA and provide controlled release of functional (antimicrobial, antioxidant, bioactives, etc.) substances, it is necessary to modify PLA's hydrophilicity, degradability, and elongation at break [61]. This can be done through bulk modifications such as adding hydrophilic and biocompatible products, or through surface modifications like adjusting surface energy, charge, and roughness [61]. For example, PLA can be copolymerized with poly(ethylene glycol) (PEG) for improved hydrophobicity, which makes the surface less attractive to proteins as well as more resistant to biological fouling and cell adhesion [61]. PLA can be synthesized through direct condensation polymerization, which produces a low molecular weight polymer but has few steps and low cost; ring opening polymerization, which uses toxic catalysts to produce high molecular weight polymers; or through enzymatic polymerization, a more environmentally friendly process that gives adequate control of the polymerization process [61]. Synthesis has energy conservation implications; Cargill Dow's methods of producing their NatureWorks™ PLA through ring opening require 25-55% less energy than required to produce petroleum based polymer with estimations of achieving 10% of energy required in the future [64]. PLA has good processing capabilities, better than poly(hydroxyl alkanoates) (PA) for example poly(hydroxybutyrate) (PHB), and can be processed using equipment used for processing petroleum-based plastic with minimum

modification [63]. PLA has demonstrated crosslinking due to electron beam radiation of dosages up to 10 kGy, however excessive irradiation, up to 30 kGy, has adverse effects due to chain scissioning on the mechanical properties such as tensile strength [65]. It degrades by hydrolysis where water, in the form of moisture, breaks down the bonds between ester monomers over the course of months [63]. Lower molecular weight varieties degrade faster than high molecular weight polymers [63].

Bacterial polyesters are thermoplastic biopolymers with wildly varying mechanical properties [58]. One such polymer, polyhydroxybutyrate (PHB), a type of poly(hydroxyl alkanoate), can be easily formed into a film [58]. It is known for biodegradability, biocompatibility, antimicrobial properties, and ease of synthesis through renewable bacteria [66]. It has mechanical properties, such as melting point, glass transition temperature, moisture barrier, and crystallinity, which are similar to industry standards such as polyethylene and polyethylene terephthalate [66]. These mechanical properties make it a prime candidate for the use in blends [66], [67]. PHB forms naturally in bacteria that have been deprived of essential nutrients in the environment. Bacteria that form these polymers include *Alcaligenes eutrophus, Pseudomonas oleovorans*, and *Protomonas extorquens* along with a variety of other similar gram-negative bacteria. These polymers are formed first by fermentation in a large vessel containing the bacteria and a source of carbon usually in the form of carbohydrates for 38-48 hours. The bacterial cells are then concentrated, dried and extracted using a hot solvent in order to purify. The polymer is then isolated using a solid-liquid separation process that removes excess cellular material and is then precipitated through the use of a nonsolvent and recovered using the solid-liquid separation process again. This process of obtaining PHB has also been done using waste products [68]. Unfortunately, there have been issues with using PHB commercially due to

the fact that homopolymer PHB is relatively brittle, and for this reason, it is often synthesized into copolymers to improve the properties [69]. For example, copolymerization of PHB and PLA has been studied as the two polymers blend to form a homogenous copolymer with improved mechanical properties over plain PHB [70]. PHB can also be copolymerized into poly(hydroxybutyrate-co-valerate), PHBV, a polymer with superior physicochemical properties, but slower degradation rates [71]. Though PHB is an attractive option, it is limited due to the fact that it costs between $4.10-$16.62 per kilogram due to the cost of the raw material and the additional price of processing the polymer from bacteria [72].

Cellulose is the most abundant naturally-occuring polymer and is found in the cell wall of many plants [52], [58], [73]. It is a fibrous, tough, water-insoluble polymer that helps to maintain the structure of the cell wall [73]. Cellulose is a promising alternative because of its renewable and low cost production, its lack of toxicity, and its biodegradability [57]. Consisting of one repeating unit, cellobiose is composed of three hydroxyl groups, which gives it hydrophobicity and biodegradability properties. It is a highly crystalline, high molecular weight polymer which normally needs to be converted to derivatives for processing [74], [75]. The hydrophobicity makes it a weak barrier for water vapor [57]. However, the biodegradation of cellulose is a slow and complicated process because of the presence of lignin, which itself can be dissolved by fungi [58]. Cellulose can be formed by the condensation reaction, composed of monomers that are joined together by glycosidic oxygen bridges [73]. The repeating unit of this polymer is a dimer of glucose, known as cellobiose [58], [73]. The sources of cellulose are preferably agricultural waste, green algae, and bacteria such as *K. xylinus* [57], [73]. Bacterial produced cellulose has a higher degree of purity, leading to increased crystallinity and mechanical properties [57]. Cellulose can be crosslinked chemically for improved properties depending on the crosslinking

agent, with glutaraldehyde used on methylcellulose leading to crosslinking associated with improved physical, thermal, mechanical, and biodegradation properties [52]. Cellophane, or regenerated cellulose, is produced from cellulose but is not used for industrial food packaging due to its high water vapor permeability [57]. The current applications of cellulose include enzyme immobilization, the synthesis of antimicrobial and medical materials, green catalysis, biosynthesis, and synthesis of drug carriers in therapeutic and diagnostic medicine [73]. Cellulose can be applied to food as coating through dipping, spraying, brushing, and panning [57]. Proper mechanical, thermal, and chemical treatment of the cellulose crystalline region can result in the formation of cellulose nanocrystals (CNCs) [52], [73]. CNC-based aerogels have attracted more attention recently for biomedical and pharmaceutical applications due to their open pore configuration and large surface area, because large quantities of drugs can be bound to the surface of CNCs [73]. CNC-containing polymer nanocomposites can be used in the production of biodegradable packaging materials to improve the mechanical performance, thermal stability, and barrier and optical properties through their improved crystallinity [73]. Solutions containing CVC and PVA can be crosslinked for improved mechanical properties [52].

Starch occurs widely in plants such as potato, corn, and rice and is one of the most inexpensive and widely available polymers [57], [58], [66]. It can even be obtained from agricultural waste products, for example plantain peels [76]. Starch can be readily processed into a low permeability film making it attractive for food packaging [58], [66]. However, this production requires starches treated with plasticizers, such as glycerol, as films made of starch alone do not have suitable mechanical and barrier properties [57], [77]. Starch is not very stable and will break down or become brittle at relatively low and/or high temperatures [58]. For the purpose of food packaging it can be enhanced through the use of nanocomposites and regular

composites [66]. Starch is attractive for our research due to its relatively low cost and the fact that it can be sustainably obtained from waste products. However, the necessity of extra processing such as plasticizers as well as the inferior mechanical properties are major drawbacks.

Gelatin is a water soluble and biodegradable polypeptide used for coatings and hydrogels [58]. It can be readily formed into a film and grafted to improve its mechanical properties [58]. Bovine bone gelatin has been crosslinked using ferulic and tannin acid for improved physical and mechanical properties [52]. Bovine hide gelatin can also be similarly crosslinked to improve its physical properties [52]. Dialdehyde carboxymethyl cellulose can be used to improve the bovine hide gelatin's optical, mechanical, and thermal properties while formaldehyde crosslinking only produces better thermal and mechanical properties [52]. Other forms of animal gelatin from fish and pigs exhibit similar improved properties depending on crosslinking agent [52].

Of the polymers presented PLA, PHB and Cellulose are the most suitable to complete our project mission. PLA is a current standard, has well established properties, is commercially producible, and has been classified as GRAS by the FDA [62], [63]. In addition, it has been shown to be modifiable both through blending, copolymerization, and crosslinking induced by radiation [61], [63], [65]. However, most aspects of PLA have been researched and there are few gaps in literature. Cellulose is very promising for low production cost and lack of toxicity [52], . However, it is hard to biodegrade, and needs mushrooms to completely degrade the polymer [58], [78]. Meanwhile, PHB has promising properties but the cost of synthesis makes it unpromising for use as a polymer backbone for our food packaging. As a result, PLA seems to be the best choice for the research being done. Crosslinking through irradiation will improve the properties, and provide a novel aspect to the project.

2.7 Plasticizers and Additives

Additives refer to any chemical added to the base polymer to improve its characteristics. Examples of additives include oxygen scavengers, antimicrobial additives, antioxidants, and plasticizers [79]. Oxygen scavengers are used to protect foods from oxidation and can be directly integrated into the walls of packaging materials [15], [80]. Antimicrobial additives prevent the growth of microbes on the polymer surface [49]. Antioxidants react with radicals and stop chain reactions [20]. Alpha-tocopherol is a natural antioxidant often incorporated into food packaging for preventing color loss, nutritional loss, and flavor changes in food [77]. Incorporating alpha-tocopherol in packaging has numerous benefits such as increased oxygen permeability, increased elongation at break, and decreased water vapor permeability [81]. However, alpha-tocopherol PLA film is twenty times more hazy than film without the additive, causing a loss in clarity [81].

Plasticizers increase the flexibility and workability of a material both internally and externally. Internal plasticizers become part of polymer molecules and reduce friction between them [82]. External plasticizers do not bond to the polymer molecules, but increase the flexibility by adjusting the properties of the polymer post polymerization [82]. Plasticizers are added to PLA to improve its mechanical properties, but they simultaneously increase the gas permeability of the material [82]. For applications in food packaging, a low oxygen gas permeability prevents oxidation and delays rancidity [83]. Plasticizers are also prone to degradation during irradiation, which can lead to migration of compounds into the food [60]. In this study, PLA without plasticizers is used in order to minimize the effect on the free radical reaction mechanisms. Triallyl isocyanurate (TAIC) is a plasticizer that has been shown to act as an effective crosslinking agent [84]. One study has shown that at radiation doses between 20 and 400 kGY

and TAIC between 3-5 wt% was optimal for inducing crosslinking [85]. In addition, use of TAIC as a plasticizer increases resistance to strain of polymer, increases tensile strength, and maintains biodegradation capabilities of the PLA polymer [84], [86].

Chapter 3

3.1 Radiation Physics

Radiation is the emission or transmission of energy in the form of waves or particles through space. As accelerating charges move through space, an electric and magnetic field is created. These fields continuously oscillate normal to the direction of the charge and are overall classified as electromagnetic radiation. Electromagnetic radiation provides heat in the form of thermal energy, creates our color spectrum, and assists in the basic metabolism of life. EM radiation has both particle and wave characteristics known as particle-wave duality. When high-energy particles and electromagnetic radiation reach a certain energy threshold they are called ionizing radiation. These energy levels are high enough to remove electrons from atoms creating unpaired electrons and positive ions which are able to further chemically react with their spatial surroundings. Ionizing radiation can be further classified as charged and uncharged and must be noted that penetration depth is proportional to initial energy levels.

Table 1.1.1 Types of Radiation and Penetration Depths

	Charged radiation		Uncharged radiation	
	Alpha particles	**Beta particles**	**Neutrons**	**Photons**
	He^{2+} nucleus	Single electrons	Single neutrons	Gamma rays X-rays High-energy UV light
Penetration depths:	Very shallow (sheet of paper)	Shallow (human tissue)	Varies with energy level	Deep - very deep (up to feet of lead)

Dr. Mohamad Al-Sheikhly, ENMA 422, "Electron Interactions with Matter"

As ionizing radiation travels through a medium, it leaves behind energy deposits from primary interactions (ionization and excitation) and secondary interactions (traveling secondary

electrons). These tracks are non-homogenous or uniform. Depending on the energy value, this can lead to blots, spurs, and short tracks and deposited energy found throughout the material. This all occurs in less than a second.

Beta particles or electron beam radiation are high-energy electrons (β^-) that can naturally be emitted by radioactive decay of an atomic nucleus during the process of beta decay Contrary to alpha particles, He^{2+}, beta particles generally have a greater ability to penetrate materials. A 0.5 MeV has a range of about one meter in air; the distance is dependent on the particle energy. At NIST, we use the electron beam accelerator Medical-Industrial Radiation Facility (MIRF). Gamma and X Rays have many similarities and often overlap each other. Both expose a targeted material to high-energy photons capable of penetrating materials deep, I.E several feet of concrete or lead. Gamma radiation is produced through the radioactive decay of an atom, usually Cobalt 60. X rays are produced within an atom's shell when an electron shifts to a low energy state causing an emission of energy we see as X rays. However, X- rays can also be produced through Bremsstrahlung Radiation. Bremsstrahlung Radiation is when high-energy electrons approach the nucleus of a target atom, attracted by its positive charge. The electric field of the atom or molecule causes the electron to de-accelerate and diverge from the nucleus. This loss of kinetic energy is what we see as X-rays., commonly used in radiography. In conclusion, we chose to continue with electron beam radiation.

3.2 Electron Paramagnetic Resonance (EPR)

Electron paramagnetic resonance (EPR) spectroscopy, also known as electron spin resonance (ESR) spectroscopy, is a powerful tool that has been used in previous literature to study the effect of radiation interaction with materials [87]–[89]. When ionizing radiation

interacts with a material, one of the degradation pathways that can occur is homolytic degradation of a sigma bond: dissociation of a chemical bond where each of the constituent atoms retains an electron, therefore including formation of two different radical species. Generally speaking, electrons may have one of two spin quantum numbers, corresponding to antiparallel spin direction: ms = -½ and ms = ½. Upon application of an external magnetic field, the energy difference between these two spin states is given by Formula 1, where g is the free radical Landé factor (g-factor) unique to the given radical species, μB is the Bohr magneton, and is the applied magnetic field strength [90].

$$\Delta E = g\mu_B\beta \quad \textbf{(1)}$$

According to the Boltzmann distribution, more free radicals occupy the lower state (ms = -½) as compared to the upper state (ms = ½). The difference in electron state occupancy is displayed in the comparison of Boltzmann factors below in Formula 2.

$$\frac{n_{upper}}{n_{lower}} = e^{-(\frac{E_{upper}-E_{lower}}{kT})} = e^{-\frac{\Delta E}{kT}} \quad \textbf{(2)}$$

At room temperature (T = 298 K), the above ratio n_{upper} / n_{lower} is approximately 0.998, therefore the transition from lower to higher energy level are more favorable. When EPR measurements are taken, microwave radiation in the X-band (with frequencies of about 9-10 GHz) is applied to the sample, and the sample absorbs a proportion of the incident radiation, thus causing some of the lower energy state free radicals to be promoted to the higher energy state. This absorption of the incident microwave radiation is used to generate an absorption signal [91].

Additionally, the resonance condition which the incident microwave radiation can provide the energy required for free radical energy state transition is given by Formula 3, where h is Planck's constant.

$$h\nu = g\mu_B\beta \quad \textbf{(3)}$$

EPR spectra are usually measured directly as first derivatives of the absorption curves, and this is accomplished using field modulation. By introducing a small (100 kHz) oscillating magnetic field, the difference in signal intensity between two successive field strength steps is measured, and through comparison to the step interval in field strength, a first derivative of signal intensity with respect to magnetic field strength can be approximated. The concept of field modulation is displayed graphically in Figure 1 below.

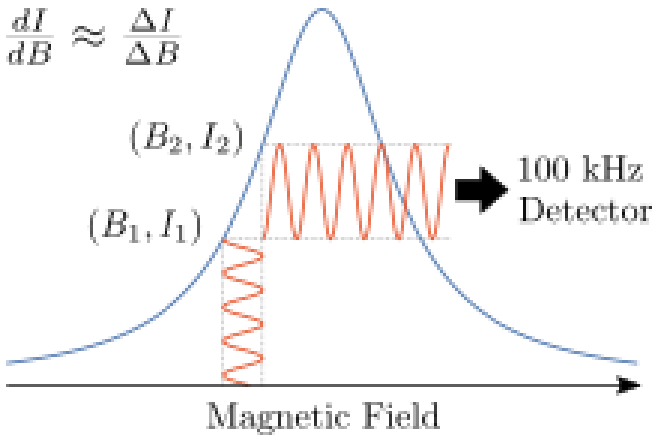

2.

Figure 1. Graphical depiction of typical field modulation (~100 kHz) in collection of single-peak representative EPR spectrum [92].

Other than the two different spin states of the free radical species, local magnetic fields due to non-zero spin nuclei must be taken into account if they are sufficiently close to the free radical species within the material structure. Because these fields can have multiple orientations with respect to that of the free radical, the EPR spectral lines may be split due to the presence of non-zero spin nuclei. In PLA, H-1 with a spin of ½ is the only non-zero spin nuclei that must be taken into account for hyperfine analysis because C-12 and O-16, the prominent isotopes of carbon and oxygen, both have spins of 0. The number of resulting peaks as a function of nearby non-zero spin nuclei is given by the Formula 4, where M is the number of equivalent nuclei splitting the radical signal, and I is the equivalent nuclei spin (e.g. ½ for H-1) [93].

$$\#\ hyperfine = \prod_i (2M_i I_i + 1) \quad \textbf{(4)}$$

EPR is used to deduce information about both the radical species and its surrounding environment. Through solving for the g-factor of a radical species, the identity of the radical species can be determined. Afterwards, through counting the number of hyperfines and solving for the number of equivalent nuclei and spin, the local environment surrounding the target radical species may be deduced, while taking into account that only non-zero spin nuclei will contribute to generation of hyperfines.

In addition to structural identification, EPR can be used to characterize the decay kinetics of the free radical concentrations. Area under the absorption curve can be directly related to the concentration of free radicals present in the sample, so through monitoring the concentration over time can lead to discovery of mechanism of interaction between the ionizing radiation and target sample, such as the competition between crosslinking and chain scission reactions.

3.3 Fourier Transform Infrared Spectroscopy (FTIR)

Fourier transform infrared spectroscopy (FTIR) is a technique used to produce an infrared spectrum of absorption or transmission of a material. Different bonds within a molecule will vibrate as a result of infrared radiation of different wavelengths. These molecular vibrations are quantized and can only vibrate at certain frequencies. In normal infrared spectroscopy, a type of absorption spectroscopy, infrared beams of one wavelength are shown through a sample and the absorption is measured. Only some bonds will have energy to absorb that light and vibrate. This can be repeated many times to get similar data to FTIR. However FTIR uses the Fourier Transform, a mathematical transform that can take the signal from a time domain and break it down to constituent frequencies. In FTIR, the dedicated computer software uses the Fourier Transform to decompose a interferogram plotting voltage versus time into a spectrum of multiple frequencies at multiple wavelengths. This allows for FTIR to shine a beam of light with multiple wavelengths of infrared at a sample. Using the Fourier transform and multiple data points comprising beams of varied wavelengths allows for the absorbance of thousands of infrared wavelengths to be found in minutes. The high peaks of absorbance occur at specific wavelengths for specific bonds, for example the C-H bond found in methyl groups absorbs infrared in the 1450 cm^{-1} range. If there are more of these bonds then that peak may be higher as more bonds are there to absorb the light of that wavelength for vibration.

3.4 Differential Scanning Calorimetry

Differential scanning calorimetry (DSC) is a technique used to study the thermal properties and transitions, such as melting, of a material. In DSC, a material sample is compared to an empty reference sample as power input is varied to keep the temperatures equal for the material and the reference samples. Temperature is then increased or decreased at a controlled

heating rate. The difference in power input required between the material and the empty reference gives the power needed to heat the material to that temperature. This difference is most commonly presented as heat flow, measured in Watts, divided by the mass of the sample. Outside of thermal transitions, this is indicative of the specific heat capacity of the material, the amount of heat required to increase one unit of mass by one unit of temperature. Plotting this specific heat flow versus temperature allows for the inference of thermal properties. During the regime outside of thermal transitions this plot has a constant heat flow value for each value of temperature; the specific heat of the material. However, during transitions, energy is required to break secondary bonds and cause phase transformations. The plot during these temperatures adopts a peak, indicating that more heat is flowing in to cause the transition without increasing the temperature of the sample. As the data is typically plotted with heat flow decreasing along the vertical axis, exothermic transitions, where heat flow is decreased due to energy released by the material, are shown as peaks and endothermic transitions, where heat flow is increased due to the extra energy required by the material for the transition, are downward facing dips in the graph. The locations of these peaks, and other characteristic behaviors indicate the transition temperatures, for example a melting point. The integration of these peaks gives the enthalpy of that transition, the energy required for it to happen.

In polymers, not all of these transitions are peaks and there are more transitions than in the metal standards typically used with DSC. Certain transitions are also only associated with certain regions within the polymer, due to the semi-crystalline nature of polymers. Going from lower temperature to higher temperature, the three transitions observed in this study were glass transition, cold crystallization, and melting.

Glass transition is due to a polymer's amorphous nature and occurs only in the amorphous segments of the polymer. At low temperatures, there is minimal vibrational energy and the molecules in a chain are “frozen” in place [94]. Mechanically, when stress is applied the polymer chains are unable to move to new positions to relieve stress; causing the material to become brittle and act glass-like. However, at the glass transition, the polymers can move more easily leading to long range segmental motion, where segments of a polymer chain can move and slide past one another resulting in the ductile behavior often associated with polymers [94]. Not only is energy required to break bonds and create vibrational movement in the polymer chains, resulting in a small peak, but the resulting heated polymer is less tightly packed and capable of movement, taking energy more readily as vibrational movement, resulting in a higher specific heat of the material past the glass transition temperature [94]. The results in an unique step-like structure to the glass transition. There are other transitions before the glass transition, such as gamma where localized bond and side chain movements begin to occur or beta, where groups of 4-8 atoms in the backbone of the polymer as well as side chains can begin to move [94]. However, these transitions are typically too small to be detected by DSC, instead leaving the glass, or alpha, transition to be the main signifier of the beginning of chain movement in DSC measurement [94].

Whereas glass transitions are associated with the amorphous region of the polymer, cold crystallization is associated with the crystalline portion of the polymer. The cold crystallization temperature is the temperature at which polymer chains gain enough energy to move into ordered, crystalline, arrangements. This, unlike the glass transition or melting, is an exothermic transition, as the chains organize themselves into more stable systems, resulting in a decrease in

the heat flow required to heat the sample a unit of temperature. The latent heat of crystallization is found by integrating this peak and can be used to calculate the crystallinity of the polymer.

Similarly to the cold crystalline transition, melting is also associated with the crystalline portion of the polymer. At the melting temperature, the crystalline portions are destroyed as the entire sample becomes amorphous and due to high temperature much more fluid. At a temperature above melting the polymer will begin to degrade, but otherwise this is a liquid as the strands of the polymer will slide against each other fluidly without ordered solid crystalline regions. This is an endothermic transition and by integrating the resulting dip in the plot you can get the latent heat of melting which can be used to calculate the total crystallinity of the sample.

The thermal properties, such as the transition points and their corresponding enthalpies can be used to compare the material to others and also, especially in the case of polymers, to calculate and infer aspects of the polymer's composition. For example, lower transition points is indicative of a lower molecular weight polymer as higher molecular weight means more dispersion forces and secondary bonds. In addition, polymer crystallinity can be determined with Formula 5 below:

$$\%X_c = \frac{(\Delta H_n - \Delta H_c)}{\Delta H^o_m} x\ 100\% \quad \textbf{(5)}$$

Where $\%X_c$ is the percentage crystallinity, ΔH_m the experimentally obtained melting enthalpy, ΔH_c the experimentally obtained cold crystallization enthalpy, and $\Delta H°_m$ a literature value calculated for the melting enthalpy of 100% crystalline polymer.

3.5 X-Ray Diffraction

X-ray diffraction (XRD) is a spectroscopic technique that can be used to quantitatively analyze the crystallinity in different types of materials, including polymers [95]–[97]. When a given material is organized into a repeating crystalline structure with an interplanar distance of d, x-rays with incident wavelength λ (e.g. 0.15406 nm for Cu Kα x-ray source) striking a source at angle θ will generate a path difference of 2dsinθ between rays diffracted from adjacent planes. Constructive interference, and thus a peak in the XRD diffractogram, will occur when the path length is an integral multiple (n) of the wavelength. This relation is encapsulated in the Bragg diffraction condition (Formula 6) which describes the conditions under which there will be constructive interference in an XRD experiment [98].

$$2dsin\theta = n\lambda \quad \textbf{(6)}$$

Because of the sinusoidal dependence on the incident angle, there is a particular resolution condition that can be reached for θ values close to 90°, which is displayed in the Formula 7 below. For a typical Cu Kα source, this corresponds to a minimum interplanar distance d of about 0.077 nm [98].

$$2d \geq \lambda \quad \textbf{(7)}$$

For highly crystalline samples, the diffraction peaks are narrow and peak locations are well-defined because the interplanar distance is relatively constant throughout the sample, so the Bragg diffraction condition occurs at well-defined incident x-ray source angles. On the other hand, peaks for amorphous samples tend to be much broader because there is much smaller long-range order in the sample, meaning smaller numbers of atomic planes will exactly meet the Bragg condition at a given angle of incidence [99]. For samples with both crystalline and

amorphous phases present, the diffractograms from each phase will add together to give one total XRD diffractogram. This type of addition is depicted in the figure below [100].

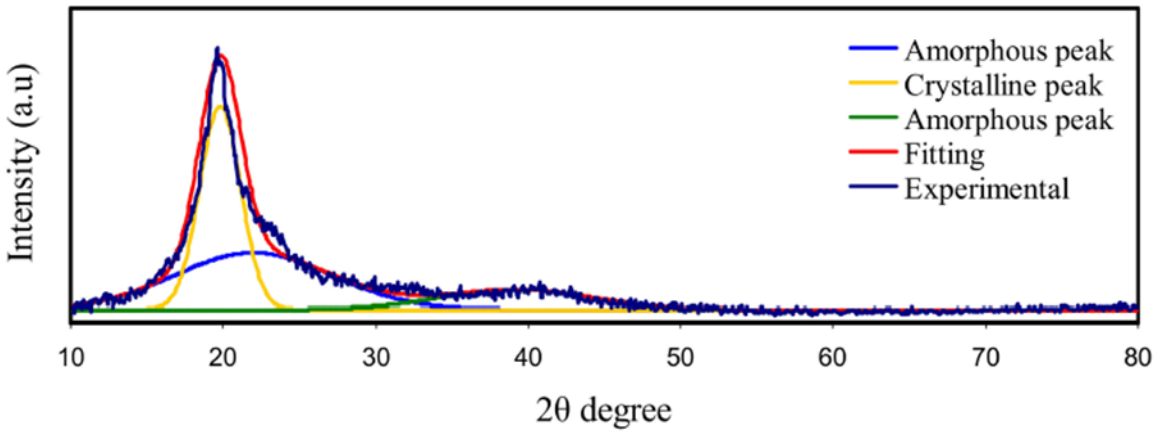

Figure 2. Experimental XRD diffractogram of pure polyvinyl alcohol (PVA) with amorphous, crystalline, and total peak fitting [100].

When used in conjunction with other characterization methods that can give information about the sample crystallinity, such as DSC, strong assertions can be made about the levels and change in crystallinity over the course of sample treatment.

3.6 Optical Microscopy

Optical microscopy was used to determine the ratio of the enantiomer within our neat PLA. The basis of optical microscopy is using visible light to see what is happening at a smaller scale using a microscope. Optical microscopy is performed with an optical microscope, which uses a series of lenses to magnify the sample. Light is shone through the sample to determine if any optical active materials are present [101].

Due to the asymmetry of the carbon within PLA, there are two different active optical states, L-oriented lactic acid monomers and D-oriented lactic acid monomers[102]. The only difference between these forms of PLA is the orientation of the groups on the carbon chain. Each form of PLA is optically active in an equal and opposite way. This means if the ratio of the racemic mixture of the enantiomers is equal, then the material is not optically active, as the PDLA and PLLA cancel out the activity of the other [102]. However, if the material is shown to be optically active, then the racemic mixture of the enantiomers is not a 50/50 mix.

3.7 Crosslinking Density

As talked about previously, crosslinking is the formation of bonds between the chains within a polymer. Crosslinking density is the way to quantify the cross links within a polymer, with high crosslinking density implying that there are many crosslinked chains within a specific volume. There are different ways to calculate the crosslinking density of polymers, namely modulus and swelling measurements. For example using the rubber-elasticity theory on thermoset, highly crosslinked, polymers to apply a mathematical model relating the storage modulus directly to the crosslinking density based on temperature. However, given that PLA is a thermoplastic with significantly different properties and much less crosslinking than a thermoset polymer, swelling tests are instead a way to calculate crosslinking density. When polymers are immersed in a solvent, swelling occurs. Solvent permeates the polymer and interacts with the polymeric network. With low enough polymer concentration in solvent, the solvent will begin to solvate the polymer chains. Crosslinking decreases the effect of swelling with its strong covalent bonds holding the polymer chains together. The degree of swelling can be measured in multiple ways. A thermomechanical analyzer (TMA) is often used to study complex moduli and thermal

properties of a material by heating the materials and measuring displacement relative to force applied. However, for a swelling experiment the temperature function can be used to keep temperature constant and prevent experimental error, the ability to apply force can be used to ensure contact between the probe and the swelling sample, and the measurement of displacement will give the amount the sample swelled.

3.8 Permeability

The permeability of a polymer is directly related to its crosslinking density. As the crosslinking density increases, the permeability of the polymer decreases [83]. This is due to an increase of pathway tortuosity within the polymer. The more tortuosity within the polymer, the more difficult the path a gas must take to to diffuse through the polymer [103]. Crosslinking increases the complexity of the polymer matrix, which increases the path complexity a gas must take to travel through the polymer. This results in more pathway tortuosity within crosslinked polymers. Testing the permeability of the irradiated polymer is needed for comparison as a food packaging material to test if post irradiation, the PLA improves its barrier properties as a packaging material. For packaging the most important gas permeability to measure is water vapor permeability as mentioned in material selection.

A gas transmittance rate is the total amount of gas transferred across the polymer over a given time, without accounting for pressure and temperature of the environment. By taking the mass difference of a container over a period of time, this is used to experimentally find the water vapor transmittance rate of our film, allowing us to see the effect of irradiation on the permeability of the gas through the sheet. Knowing the WVTR of our irradiated PLA allows us to assess its possible use as a food packaging material.

3.9 Tensile Testing

Tensile testing is a destructive measurement designed to determine the mechanical properties of a material. In the scope of this project, tensile testing was done in tension, in which the material was pulled in opposite directions until break to determine properties. The testing machine measures the force exerted and its own displacement. The result of this is given in displacement (ΔL) and force (F) which then can be used to determine engineering stress (σ) and strain (ε) using the cross-sectional area of the sample (A) and the total length of the sample (L) under load.

$$\sigma = \frac{F}{A} \quad \textbf{(8)}$$

$$\varepsilon = \frac{\Delta L}{L} \quad \textbf{(9)}$$

These two measurements are used to construct a stress-strain plot from which many mechanical properties can be determined. When solid materials are subjected to only small stress, then the elongation is due to the stretching of the bonds between atoms [104]. This results in a linear relationship between stress and strain. Because this displacement is due to the stretching of bonds, the material is still capable of returning to its original position in reversible deformation. As a result this mode of deformation is called “elastic deformation.” At higher stresses, the planes of atoms begin to slip past one another in irreversible deformation. This deformation is called “plastic deformation.” For most materials, the initial elastic deformation appears as linear. The slope of that portion is called the Young’s modulus or elastic modulus (E). The stress at which the material yields and begins to permanently deform is called the yield strength (σ_y).

Typically, the end of this elastic region at the yield strength is hard to determine. As a result, one method to determine an engineering yield strength is to construct a parallel line to the

linear region at an offset strain. The point at which this offset line intersects the stress strain curve can be used as the yield strength and is typically called the offset yield strength. The typical offset used is 0.2%. After the yield strength, the polymer begins to plastically deform moving chains against one another. As more and more chains are moved it becomes more and more difficult to move resulting in a non-linear increase in stress. The ultimate tensile strength is the highest stress experienced by the sample over the course of the test. Typically with polymers, this is associated with beginning of necking in which the polymer chains within the sample align, reducing cross-sectional area. As all calculations are done using an initial measured value of the cross-section, the strain measured will be less than the true strain and as a result what would be near constant is shown as a reducing trend in stress. The elongation at break is the final strain value before the sample breaks.

Due to the use of stress and strain these measurements can be used to compare with other materials as they are not influenced by the size and length of the sample. A summary of these properties can be found in the following typical stress-strain curve.

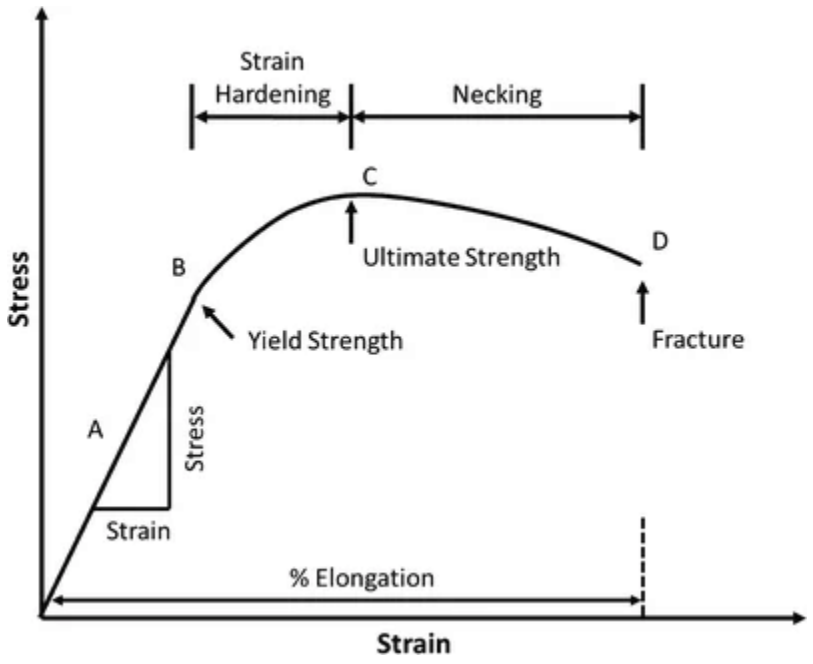

applied sciences

MDPI

Article

On the Mechanism of Electron Beam Radiation-Induced Modification of Poly(lactic acid) for Applications in Biodegradable Food Packaging

Eleanor C. Grosvenor [1], Justin C. Hughes [1], Cade W. Stanfield [1], Robert L. Blanchard [1], Andrea C. Fox [1], Olivia L. Mihok [1], Kristen Lee [1], Jonathan R. Brodsky [1], Ann Hoy [1], Ananya Uniyal [1], Sydney M. Whitaker [1], Chris Acha [1], Kalina Gibson [1], Lilly Ding [1], Catherine A. Lewis [2], Lorelis González López [2], Charlotte M. Wentz [3], Lawrence R. Sita [3] and Mohamad Al-Sheikhly [2,*]

[1] Gemstone Honors Program, University of Maryland, College Park, MD 20742, USA; egrosven@terpmail.umd.edu (E.C.G.); jhughes3@umd.edu (J.C.H.); cstanfie@termpail.umd.edu (C.W.S.); rblancha@umd.edu (R.L.B.); afox1234@terpmail.umd.edu (A.C.F.); omihok@terpmail.umd.edu (O.L.M.); klee323@terpmail.umd.edu (K.L.); jbrodsky@umd.edu (J.R.B.); ahoy1@terpmail.umd.edu (A.H.); auniyal@umd.edu (A.U.); swhitak1@umd.edu (S.M.W.); cachangw@umd.edu (C.A.); kgibson0@terpmail.umd.edu (K.G.); lding1@terpmail.umd.edu (L.D.)

[2] Department of Materials Science and Engineering, University of Maryland, College Park, MD 20742, USA; clewis12@terpmail.umd.edu (C.A.L.); lorelis@terpmail.umd.edu (L.G.L.)

[3] Department of Chemistry and Biochemistry, University of Maryland, College Park, MD 20742, USA; cwentz@terpmail.umd.edu (C.M.W.); lsita@umd.edu (L.R.S.)

* Correspondence: mohamad@umd.edu; Tel.: +1-(301)-461-4348

Citation: Grosvenor, E.C.; Hughes, J.C.; Stanfield, C.W.; Blanchard, R.L.; Fox, A.C.; Mihok, O.L.; Lee, K.; Brodsky, J.R.; Hoy, A.; Uniyal, A.; et al. On the Mechanism of Electron Beam Radiation-Induced Modification of Poly(lactic acid) for Applications in Biodegradable Food Packaging. *Appl. Sci.* **2022**, *12*, 1819. https://doi.org/10.3390/app12041819

Academic Editors: Dorota Swiatla-Wojcik, Yosuke Katsumura, Radosław A. Wach and Ramona Iseppi

Received: 4 November 2021
Accepted: 28 January 2022
Published: 10 February 2022

Featured Application: Electron beam radiation induces C-O-C bond scissions on the backbone of the amorphous poly(lactic acid) (PLA) used for food packaging. The radiolytically produced alkoxyl radicals abstract hydrogen atoms from the neighboring PLA molecules, leading to the formation of carbon-centered radicals. Since all PLA samples were exposed to air after irradiation and electron paramagnetic resonance (EPR) measurements, the carbon-centered radicals react with oxygen to form the corresponding peroxyl radicals. The resultant PLA is suitable for food irradiation and is biodegradable after the packaging is discarded. The radiation of sterilization has no detrimental effect on the water vapor diffusion through the PLA membrane.

Abstract: Poly(lactic acid) (PLA) is a biodegradable polymer used for food packaging. The effects of electron beam radiation on the chemical and physical properties of amorphous PLA were studied. In this study, amorphous, racemic PLA was irradiated at doses of 5, 10, 15, and 20 kGy in the absence of oxygen. Utilizing electron paramagnetic resonance spectrometry, it was found that alkoxyl radicals are initially formed as a result of C-O-C bond scissions on the backbone of the PLA. The dominant radiation mechanism was determined to be H-abstraction by alkoxyl radicals to form C-centered radicals. The C-centered radicals undergo a subsequent peroxidation reaction with oxygen. The gel permeation chromatography (GPC) results indicate reduction in polymer molecular mass. The differential scanning calorimetry and X-ray diffraction results showed a subtle increase in crystallinity of the irradiated PLA. Water vapor transmission rates were unaffected by irradiation. In conclusion, these results support that irradiated PLA is a suitable material for applications in irradiation of food packaging, including food sterilization and biodegradation.

Keywords: electron beam radiation; poly(lactic acid); alkoxyl free radical decay

1. Introduction

Every year, 1.3 billion tons of food are wasted globally [1,2]. This figure corresponds to almost one third of all food produced for humans [2]. In theory, global food production can provide for every living person, indicating that ineffective food distribution systems are

substantial contributors to world hunger [3]. According to the United States Department of Agriculture, 31 percent of U.S. food supply at the retail and consumer levels is wasted [4]. Of the United States' total food waste, packaging accounts for 29.5% of municipal solid waste, suggesting that a more efficient material for the transport and storage of foods may contribute to less food wasted [5]. Simultaneously, our waste management systems face an overwhelming influx of discarded plastic products [6]. Even so-called recyclable materials have a limited number of cycles before they undergo phase separation and become unusable, meaning that recycling is not an effective solution to plastic waste [7].

A solution to both food spoilage and plastic waste is a biodegradable polymer that extends the shelf life of produce through selective permeability of the membrane. Currently, finding an appropriate bio-based polymer can be rather challenging because they are typically hydrophilic in nature, leading to high water vapor transmission rates [8,9]. The concentrations of oxygen gas and water vapor must remain low to prevent spoilage due to oxidation [10,11]. Within the localized packaging environment, a modified, carbon dioxide-rich environment is necessary to preserve food and delay rancidity [12–14]. Carbon dioxide maintains a low pH, which decreases microbe growth [12–14].

A polymer capable of the aforementioned tasks is poly(lactic acid) (PLA). PLA is a polyester that is classified as Generally Recognized as Safe (known as GRAS) by the U.S. Food and Drug Administration [15]. Commercial synthesis of PLA via the condensation of lactic acid is an environmentally friendly, inexpensive, and energy efficient process [16–21]. For these reasons, PLA has been established as a viable biodegradable polymer for food packaging applications [22–27]. PLA has two naturally occurring stereoregular forms, PDLA and PLLA [28]. A great deal of current research is focused on characterizing these forms with techniques such as nuclear magnetic resonance [29]. A racemic mixture of PLA leads to an amorphous polymeric structure [28]. The water vapor permeability of the racemic PLA is 14–23% lower than for the homopolymers, making racemic PLA an ideal choice for food packaging applications [30]. Moreover, dipole–dipole interaction and hydrogen bonding between the two stereoregular forms lead to a stronger, denser material with improved thermal stability [30].

Food packaging is inextricably linked to radiation in multiple ways. First, ionizing radiation is already utilized as a safe method of extending shelf life and ensuring the safety of food products [31]. Food is irradiated inside its packaging once it is ready for retail, and this process serves several purposes including the delay of sprouting and ripening, reduction of spoilage-causing organisms, control of insects, and the prevention of foodborne illness through elimination of pathogenic bacteria [31,32]. Electron beam radiation for the treatment of fruits and vegetables is typically achieved with doses up to 10 kGy [31]. After the consumer has discarded the food packaging, radiation is used to enhance the slow biodegradation rate of PLA [33].

Elucidating the radiation chemistry mechanism of PLA via identification of the radiolytically produced free radicals and their decay will further the understanding of the physical properties, permeability, and biodegradability of PLA. It is expected that radiation-induced C-O-C bond scissions in the PLA will occur under the radiation conditions used in this work.

Previous research showed that the molar mass of PLA decreased when irradiated at 25 °C compared to an increase in molar mass at 80 °C and 170 °C [34]. Malinowski states that crosslinking of PLA is optimized at a dose of 40–200 kGy and 3–5 wt% triallyl isocyanurate (TAIC) additive [35]. Chain scission is the primary reaction when neat PLA is irradiated from 1–100 kGy [36]. As a result of irradiation, the gel fractions were between 0.5% and 0.9%, the heat of fusion increased, and the glass transition temperature decreased slightly, all indicating the presence of chain scission and a reduction in molar mass [36]. The chain scission occurs predominantly at the C-O-C bonds on the backbone of the PLA chain [37,38].

Electron beam radiation in the range of 1 to 30 kGy in the presence of oxygen prompts PLA degradation; a decrease was seen in the molar mass, tensile strength, break elongation

and elastic modulus, and water vapor permeability of the polymer [39]. Another group found that electron beam irradiation at doses below 25 kGy did not cause any changes in the mechanical properties of PLA [40]. PLA has a resistance to radiation treatment that adds to its potential for applications in food packaging [40]. Another group observed that the degree of crystallinity for poly-L-lactic acid increased with dose up until 50 kGy [33]. Overall, the previous literature shows varied results depending on the irradiation conditions. For the scope of this research, samples were irradiated at doses of 5, 10, 15, and 20 kGy in the absence of oxygen.

2. Materials and Methods

2.1. Background on Material Used in Experimentation

A commercial-grade sheet of polylactic acid was graciously donated by Ex-Tech Plastics. The PLA sheets were approximately 25.4 cm × 20.3 cm with a thickness of 0.0304 cm. The material was identified and characterized as received using optical microscopy (Olympus BX40 microscope, Tokyo, Japan), X-ray diffraction (XRD) (Rigaku Miniflex 600 with D/teX Ultra silicon strip detector, Tokyo, Japan), Fourier transform infrared spectroscopy (FTIR) (Nicolet iS50 FTIR spectrometer, Thermo Scientific, Waltham, MA, USA), differential scanning calorimetry (DSC) (DSC Q100, TA Instruments, New Castle, DE, USA), and gel permeation chromatography (GPC)(VE 2001 GPCMax, Viscotek, Houston, TX, USA). The L and D composition of the amorphous PLA was determined to be racemic after analysis of optical microscope images. We used XRD to confirm that we had highly amorphous PLA, as shown in Figure 1 by the two wide peaks and no sharp peak corresponding to a crystalline phase. We explain these results in detail in Section 3.5. We subsequently performed GPC and obtained a number average molar mass (M_n) of 119,500 Da, weight average molar mass (M_w) of 196,400 Da, and polydispersity index of 1.646 for the unirradiated PLA samples. As shown in Figure 1, DSC results demonstrated that the material is not a stereocomplex, but rather a copolymer of P(DL)LA with equal proportions of L and D subunits. The double melting peak due to stereocomplexation would occur at a higher temperature than we observed, indicating that the double peak in our DSC results can be attributed to perfected spherulites. We expand on this analysis in Section 3.3. PLA without plasticizers and additives is used, as confirmed by FTIR spectral analysis on unirradiated PLA, shown in Figure 1 and analyzed in Section 3.2.

2.2. Optical Microscopy

Optical microscopy was utilized to determine the L and D composition of the PLA. Microscope images were taken on the Olympus BX40 microscope (Japan), both with and without polarized light. The objectives used were 4×, 10×, and 40×. Prior to optical microscopy, the PLA was spin coated to prepare a thin polymer film. The PLA samples were dissolved in dimethyl sulfoxide at a concentration of 8 mg/mL. The spin coater was run for 30 s at 3000 rpm to deposit the solution onto a silicon wafer.

2.3. Sample Preparation and Irradiation

The sheets of PLA were cleaned with deionized water and cut into two different-sized pieces for sample treatment, the smaller being 52 mm × 4 mm and the larger being 52 mm × 16 mm. The 52 mm × 4 mm sample was used for electron paramagnetic resonance (EPR) characterization, while the 52 mm × 16 mm sample was divided between FTIR and water vapor transmission rate (WVTR) testing. FTIR is a non-destructive test, and it was performed before the WVTR tests. Each pair of small and large PLA strips was placed into an individual 40 mL septum vial and purged at 7 psi for 20 min with inert gas, which was either nitrogen or argon. These septum vials were then sealed with parafilm prior to irradiation.

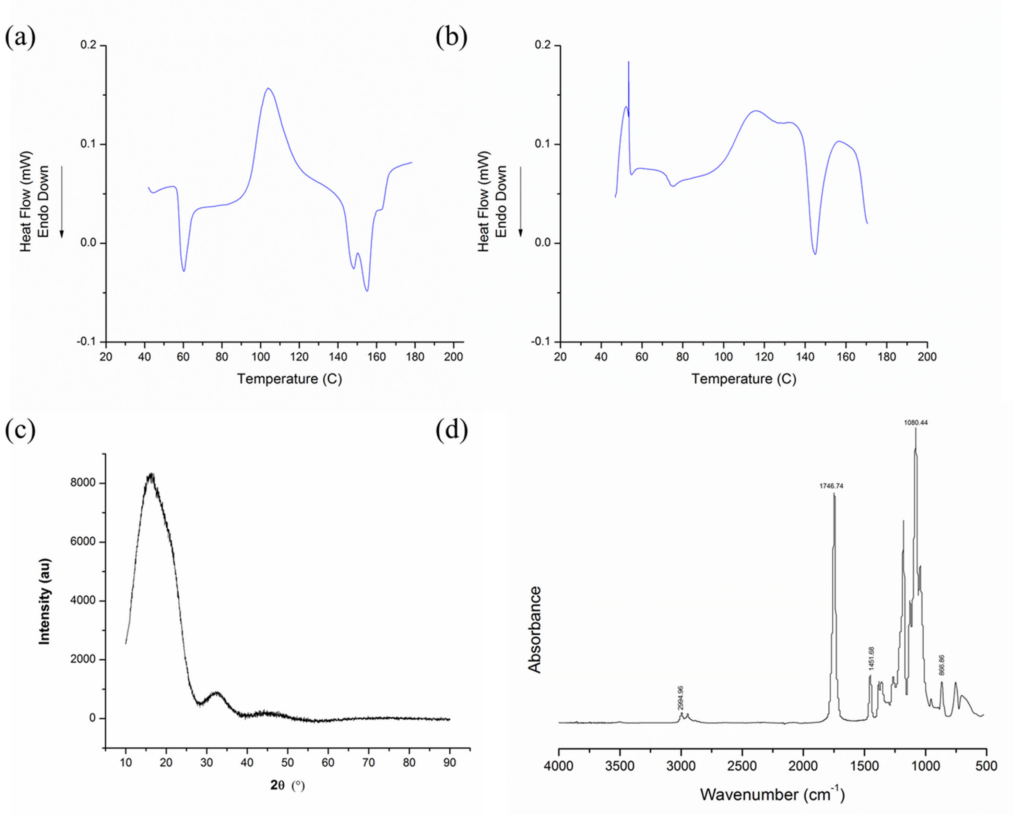

Figure 1. Characterization of unirradiated PLA. (**a**) Average DSC cycle 1; (**b**) average cycle 2; (**c**) XRD diffractogram; (**d**) FTIR spectra (labels: 2994.96, 1746.74, 1451.68, 1080.44, 866.86 cm^{-1}).

Irradiation was conducted at the Medical Industrial Radiation Facility at the National Institutes of Standards and Technology Physical Measurement Laboratory using a Sagattaire traveling-wave electron linear accelerator. The pulse width was maintained at 6 µs with a pulse repetition of 100 pulses/s and an energy of 11.5 MeV. The samples were irradiated to a total dose of 5, 10, 15, and 20 kGy and at an average dose rate of 68 kGy/h. Dosimetry was conducted using strips of alanine placed in the path of the electron beam. Samples were placed on a foam block 100 cm from the exit beam. The electron beam was run at room temperature. Once irradiated, the samples were kept on dry ice in the absence of oxygen prior to transfer from septum vials to EPR tubes for subsequent EPR analysis. This sample transfer was conducted in a glove box purged with nitrogen at 7 psi.

2.4. Radical Structure and Concentration Decay Characterization Using Electron Paramagnetic Resonance (EPR) Spectrometry

2,2-diphenyl-1-picrylhydrazyl (DPPH) was used to calibrate the frequencies from the microwave generator, and EPR measurements were taken for each of the irradiated samples. DPPH was chosen as it contains a stable free radical which is possible through stabilization provided by the three rings in its structure. The following instrument parameters were used: microwave power of 5 mW, frequency modulation of 100 kHz, modulation amplitude of 3.12 G, receiver gain of 6.32×10^3, center field at 3500 G, sweep width of 1000 G, conversion time of 40.96 ms, and time constant of 20.48. The parameters were selected to avoid overmodulation or signal distortion, and four sweeps over the magnetic field spectrum were conducted for each sample to maintain a high level of signal resolution. The expected number of hyperfines for an EPR spectrum can be described by Equation (1):

$$number\ of\ hyperfines = \Pi 2 n_i I_i + 1 \quad (1)$$

where n_i denotes the number of equivalent nuclei and I_i denotes the nuclear spin of the equivalent nuclei. The concentration of radicals in spins per gram was determined from Equation (2):

$$[x] = \frac{[std]A_x R_x (scan_x)^2 G_{std} M_{std} (g_{std})^2 [s(s+1)]_{std}}{A_{std} R_{std} (scan_{std})^2 G_x M_x g_x^2 [s(s+1)]_x} \quad (2)$$

where $[x]$ denotes radical concentration, A_x denotes the double integral of the EPR first derivative curve, $scan_x$ denotes the magnetic field sweep width in gauss, G is the gain of the signal amplifier (Hz), M is the modulation amplitude (G), g is the Lande factor, s is the radical spin quantum number, and R is the Kramers degeneracy of the EPR spectrum. The subscript *std* refers to the parameters measured from the manganese sulfate monohydrate ($MnSO_4 \cdot H_2O$) standard sample and the subscript x refers to the parameters measured from the experimental samples.

2.5. Bond Structure Characterization via Fourier Transform Infrared Spectroscopy (FTIR)

FTIR spectroscopy was used to measure the oxidation index of the irradiated samples. Infrared spectra of PLA samples were taken on the Thermo Scientific Nicolet iS50 FTIR spectrometer (USA) from 525–4000 cm^{-1} with a resolution of 4 cm^{-1} and analyzed via the OMNIC software. An attenuated total reflectance (ATR) accessory, the SmartiTx with diamond, was used. Ninety-six scans at a resolution of 4 cm^{-1} were performed for each spectrum to obtain averages, and two spectra were taken per sample. Backgrounds were taken every 30 min, and the changes in peaks were analyzed thereafter. All FTIR spectra were normalized to the peak at about 1450 cm^{-1} corresponding to the C-H stretching in the methyl groups. This was done by dividing the range of absorbance values from 500 to 4000 cm^{-1} by the absorbance at 1450 cm^{-1}. The C-H stretch at 1450 cm^{-1} was chosen due to the expected lack of change in C-H bonds in methyl groups as a result of irradiation [41]. FTIR was used to calculate the oxidation index for C-O and C=O bonds. Integrals of the C-O peak at approximately 1100 cm^{-1}, C=O peak at approximately 1750 cm^{-1}, and CH_3 peak at approximately 1450 cm^{-1} were calculated using the Origin8 Software. Oxidation index for the C-O and C=O peaks was found by dividing the integrated area of their respective peaks by the integrated area of the CH_3 peak, the reference peak.

2.6. Thermal Analysis Using Differential Scanning Calorimetry (DSC)

DSC analysis was performed on samples of about 5 mg in sealed aluminum pans in a nitrogen atmosphere using a TA Instruments DSC Q100 (USA). The samples were subjected to two heating and cooling cycles. In the first run, the samples equilibrated at 40 °C and then increased to 190 °C. They were held isothermal for five minutes at 190 °C before being cooled back down to 40 °C. The samples were again held isothermal for five minutes at 40 °C before increasing to 190 °C, where they were held isothermal for five minutes. Finally, the samples were cooled to 40 °C. For both heating cycles, the scanning rate was 5 °C min^{-1}. From the resulting thermograms, attempts were made to measure the glass transition temperature (T_g), cold crystallization temperature (T_c), cold crystallization enthalpy (H_c), melting temperature (T_m), and melting enthalpy (H_m). Despite the fact that the unirradiated PLA samples were almost completely amorphous, efforts were made to measure the percent crystallinity ($\%X_c$) using Equation (3) after irradiation in case any crystallization had occurred in the irradiated samples:

$$\%X_c = \frac{\Delta H_m - \Delta H_c}{\Delta H^\circ_m \times 100} \quad (3)$$

where H_m is the experimentally determined melting enthalpy (Jg^{-1}), H_c is the experimentally determined cold crystallization enthalpy (Jg^{-1}), and H_m is the melting enthalpy for 100% crystalline PLLA, stereoregular L-oriented PLA (93 Jg^{-1}) [42].

2.7. Characterization of Crystallinity with X-ray Diffraction (XRD)

XRD diffractograms (Rigaku Miniflex 600 with D/teX Ultra silicon strip detector, Japan) were taken for an unirradiated and a 20 kGy irradiated sample two weeks post-irradiation to confirm equilibrium crystallinity of the polymer samples. The measurements were conducted using 2θ values between 10° and 90° with a step size of 0.2°, and a Rietveld refinement based on an SI standard was conducted to analyze diffracted peak locations.

2.8. Gel Permeation Chromatography (GPC)

GPC was used to obtain molar mass (M_n and M_w) and polydispersity index (PDI) of PLA films using Viscotek VE 2001 GPCMax (USA) equipped with three columns (Styragel HR-4, HR-3, and HR-1) in a column oven and differential refractometer (maintained at 40 °C). Tetrahydrofuran (HPLC grade) was used as the eluent with a flow rate of 1 mL/min. Polystyrene standards (from Polymer Laboratories Inc., 580 Da–3039 kDa) were used for calibration. For GPC sample preparation, 2–4 mg of dry PLA film sample was dissolved in 2 mL of THF (HPLC grade).

2.9. Water Vapor Transmission Rate (WVTR) Testing

Materials included a 40 mL septum vial, a desiccant (2–5 mm silica beads), fume hood, a balance showing uncertainty to four decimal places (±0.0001 g), adhesive silicone or other water-resistant sealant, and the testing material: a sheet of PLA with a width of 0.0304 cm. The scale used was a New Classic MF model MS105DU, produced by Mettler Toledo. The following methodology is a modified version of ASTM Standard E96: Standard Test Methods for Water Vapor Transmission of Materials [43]. PLA was cut from a sheet to completely cover the surface area of the opening of the 40 mL septum vial. The septum vial was weighed, and the initial weight was recorded. The silica beads were added to the vial and filled to within 1/2 inch of the top of the vial. The weight of the vial with the additional silica beads was measured. The PLA sample was then attached to the top of the vial using the silicone sealant. A continuous layer of sealant was applied to the edges of the top of the vial, and the sample was pressed to the sealant and allowed to dry. The vial was weighed again for the initial testing weight and placed in the test chamber. After initial weighing, the sample was weighed once every day for the following six days. The weight of the vial was plotted over time. WVTR was calculated using Equation (4):

$$WVTR = \frac{G}{t \times A} \quad (4)$$

where G is the weight change in grams, t is time in days, and A is the test area of the vial mouth in meters squared. $WVTR$ is measured in $gd^{-1}m^{-2}$.

3. Results and Discussion

3.1. Identification of the PLA Radiolytically Produced Free Radicals and Their Kinetics Decay

Representative EPR spectra from each of the four doses were taken for comparison and plotted in Figure 2. Upon examination of each of the spectra, it is apparent that the dominant splitting pattern is four peaks with relative intensity magnitudes of 1:3:3:1. Assuming interactions between atoms less than three bond-lengths away from the radical contribute to the hyperfine structure, this splitting pattern matches the predicted result from Equation (1). H-abstraction from PLA results in three equivalent hydrogen atoms located two bond-lengths away from the carbon-centered radical. Substitution of $n = 3$ for the number of equivalent hydrogen atoms and $I = 1/2$ for the nuclear spin of hydrogen yields four hyperfine peaks, which is in agreement with experimental results.

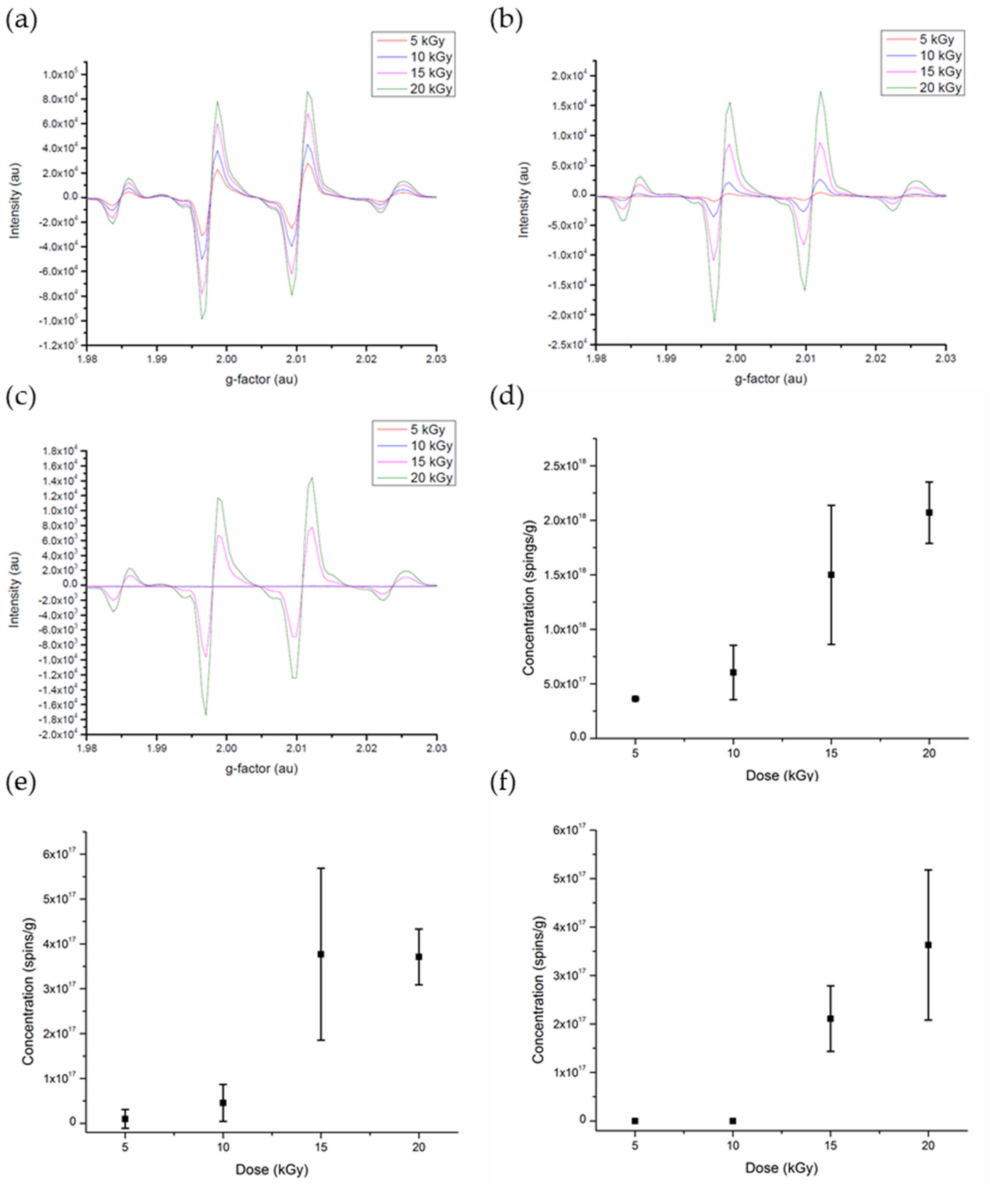

Figure 2. (**a**–**c**) Time series of EPR spectra for PLA irradiated at 4 different doses: 5 kGy (red), 10 kGy (blue), 15 kGy (pink), and 20 kGy (green). There were three time points used: (**a**) same day as irradiation (day 0); (**b**) day following irradiation (day 1); (**c**) second day following irradiation (day 2). (**d**–**f**) Dose–yield plots over the first three days. These measurements were taken twice at 5 kGy, twice at 10 kGy, four times at 15 kGy, and twice at 20 kGy**.** (**d**) Day 0; (**e**) day 1; (**f**) day 2.

This dose dependence can be further expanded upon by calculating the number of radicals present in the sample over time, with concentration expressed in spins per gram. Figure 3 illustrates this calculation. Even on day 2, in the absence of oxygen, relatively stable free radicals are still present. We believe it is a mixture of alkoxyl radicals, including radical (b) in the proposed mechanism of Figure 4. After one week, the radical concentration had decreased below the effective detection limit of the spectrometer and all yields were approximately zero spins per gram. For the reactions that occur after the irradiation of PLA, the rate-determining step is the abstraction of hydrogen by alkoxyl radicals. The decay fits neither first nor second order reaction kinetics due to complexity of the free radicals present.

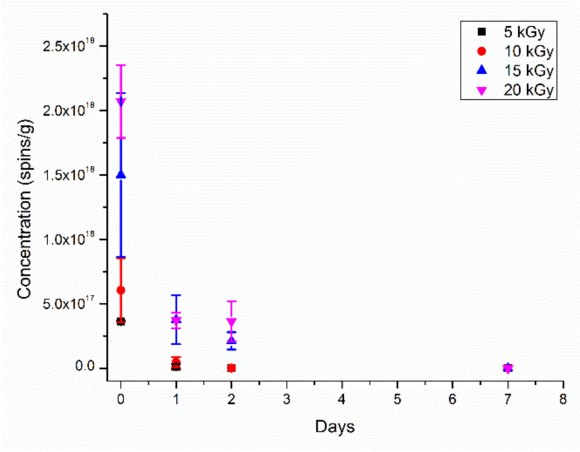

Figure 3. Time dependence radical concentration decay for PLA samples after irradiation at 5 kGy, 10 kGy, 15 kGy, and 20 kGy. The values at day 0 on the x-axis correspond to spectra that were taken a couple of hours after irradiation and kept in dry ice.

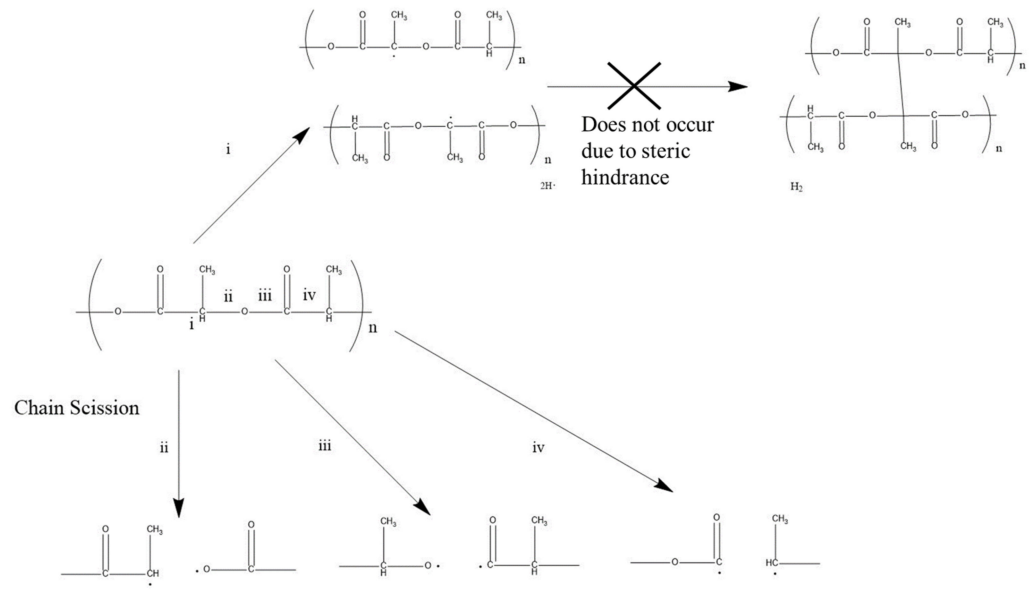

Figure 4. Proposed mechanism for chain scission of PLA after electron beam irradiation.

Figure 4 shows the overall proposed reaction mechanisms of the radiolysis of PLA in the absence of oxygen. The EPR results demonstrate the radiation-induced C-O-C bond scissions that lead to the formation of the oxidative alkoxyl radicals and the reductive C-centered radicals. The alkoxyl radicals abstract H atoms from the neighboring molecule, giving rise to the formation of more C-centered radicals. The carbon-centered radicals on nearby PLA chains are not expected to undergo crosslinking reactions (reaction pathway i) because of steric hindrance. After chain scission (reaction pathways ii and iii), the alkoxyl radical abstracts a hydrogen from an adjacent polymer chain, giving rise to the formation of C-centered radicals. In addition, alkoxyl radicals undergo β-fragmentation and 1,2-H-shift reactions [44]. Since oxygen is not present during the EPR measurements only, the peroxyl radicals are not expected to be present, thus limiting the potential for chain scission [37]. In this investigation, dry ice was used to slow radical concentration decay kinetics until they could be characterized by EPR, and the inert atmosphere was used to prevent the formation of undesired radical species, such as the peroxyl radical, that could impact the resultant PLA structure. As expected, the presence of the L and D stereoregular forms of PLA shown in Figure 5 did not impact the shape of the EPR spectra.

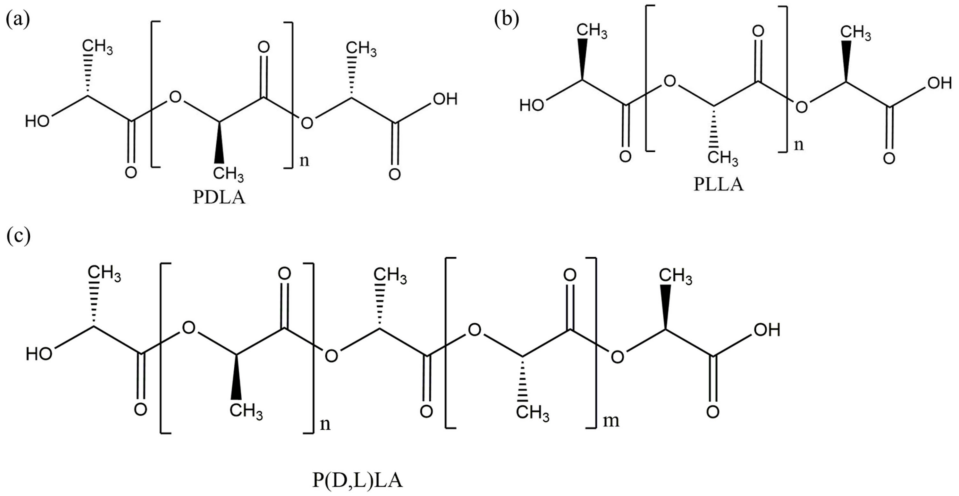

Figure 5. Stereoregular forms of PLA: (**a**) poly-D-lactic acid; (**b**) poly-L-lactic acid; (**c**) copolymer of P(DL)LA with equal proportions L and D subunits.

3.2. Oxidation Index Based on FTIR Spectroscopy

The characteristic absorption bands of each PLA functional group were found, corresponding to what is expected in the literature [45–48]. As shown in Figure 6, every spectrum contains an absorption band just below 3000 cm^{-1} corresponding to the C-H stretch and a weaker band at 1250 cm^{-1} corresponding to C-H deformation. Spectra also contain an absorption band around 1750 cm^{-1} for the C=O stretch, and weaker bands at 1380 cm^{-1} and 770 cm^{-1} correspond to the C=O bend. The absorption band near 1450 cm^{-1} corresponds to the CH_3 bend, and the intense absorption bands in the 1180 and 1080 cm^{-1} range are representative of the C-O stretch. The absorption band at 1040 corresponds to the OH bend. The absorption bands around 860 cm^{-1} correspond to C-C stretches.

FTIR spectroscopy was used primarily to determine the oxidation index (OI) in the irradiated samples (Table 1). OIs which include the formation of aldehydes, ketones, and carboxylic groups were found to increase with irradiation for all doses. Although these samples were irradiated in the absence of oxygen, they were exposed to the air after irradiation. Therefore, it is expected that peroxidation of the free radicals will take place.

Table 1. The OIs of the C-O bond, using the peak at approximately 1100 cm^{-1}, and the C=O bond, using the peak at approximately 1750 cm^{-1}. Calculated using the CH_3 peak at approximately 1450 cm^{-1} as a reference [49].

Sample	Oxidation Index of C-O	Oxidation Index of C=O
Unirradiated	6.27 ± 0.13	15.4 ± 0.31
5 kGy	6.64 ± 0.13	18.5 ± 0.37
10 kGy	7.57 ± 0.15	20.1 ± 0.40
15 kGy	6.97 ± 0.14	18.4 ± 0.37
20 kGy	7.24 ± 0.14	18.0 ± 0.37

3.3. DSC Results

The thermal behavior of the unirradiated and irradiated samples from the thermal analysis is given in Table 2. The glass transition of unirradiated samples was 60.8 ± 1.2 °C on average. Therefore, the samples were in a glassy phase during irradiation. Since the total dose used in this study was comparatively low, as a result, the degradation was minimal and there was no effect on T_g.

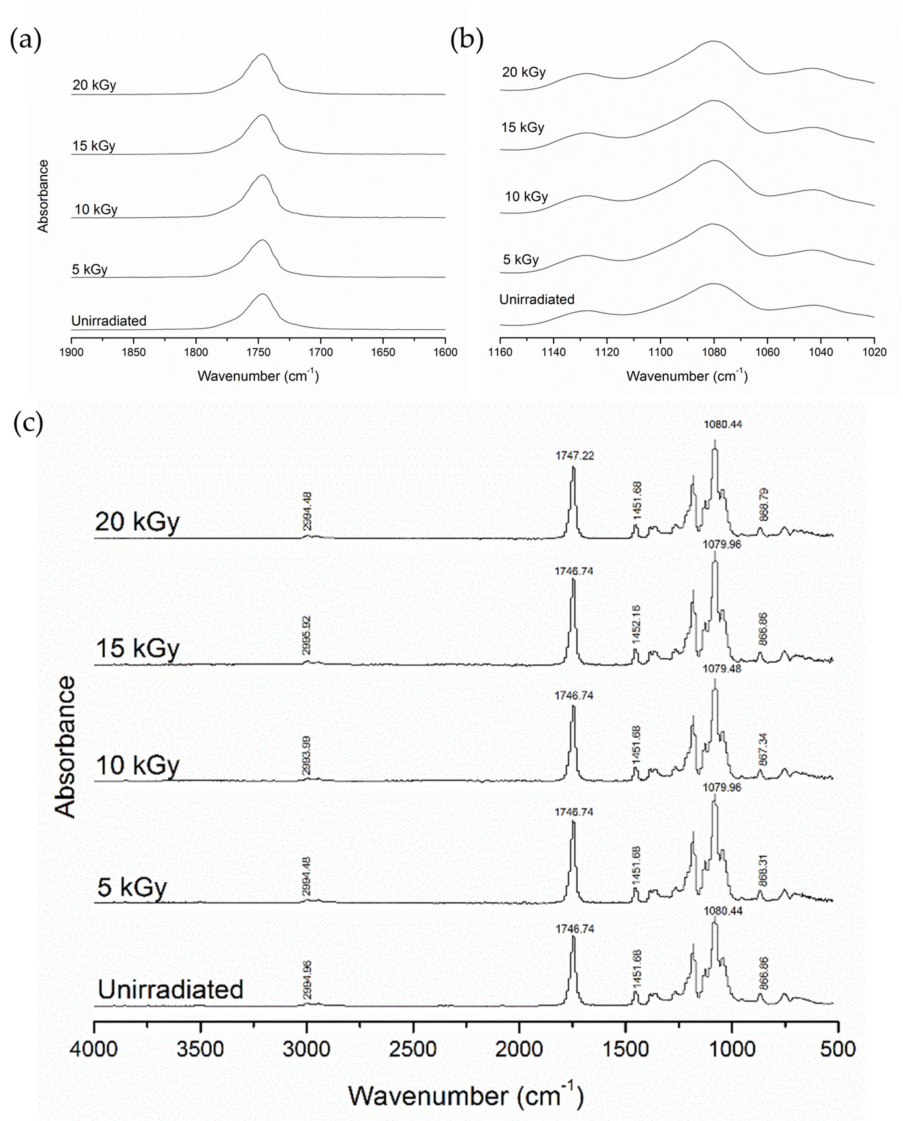

Figure 6. FTIR spectra from samples irradiated at 0, 5, 10, 15, and 20 kGy in the absence of oxygen, followed by exposure to air after irradiation. (**a**) Comparison of spectra within the range of the C=O peak; (**b**) comparison of spectra within the range of the C-O peak; (**c**) full spectra.

Table 2. Average values of key thermal properties and crystallinity changes as a function of irradiation dose, calculated using DSC spectra obtained from the second heating cycle.

Sample	Glass Transition (°C)	Softening Point (°C)	Percent Crystallinity (%)
Unirradiated	60.8 ± 1.2	153.3 ± 2.2	1.2 (negligible)
5 kGy	59.6 ± 0.7	152.3 ± 1.5	2.4 ± 0.12
20 kGy	59.5 ± 0.9	151.2 ± 0.8	7.3 ± 0.4

The cold crystallization and softening points were found to be on average 122.1 ± 1.7 °C and 153.3 ± 2.2 °C, respectively. The average transition temperatures for irradiated samples slightly decreased with increasing dose due to chain scissions resulting in shorter chains. A negligible ratio of crystallinity was found to be 1.2% on average in unirradiated samples. With increasing radiation dose, an increase in crystallinity was observed, with crystallinity of 2.4 ± 0.12% at 5 kGy and 7.3 ± 0.4% at 20 kGy. A larger increase in crystallinity was expected [35]. However, the steric hindrance on the backbone of the PLA chains impeded crystallization of these broken chains.

As shown in Figure 7, a pronounced double melting peak was observed in the first heating cycle, with the two peaks occurring at approximately 155 °C and 161 °C. The stereocomplex consisting of both PLLA and PDLA has a higher melting point than tactically pure PLA due to interlocking of oriented chains [50]. A double peak due to stereocomplexation would be found around 220 °C, much higher than the second peak we observed [50–52]. Therefore, it is more likely that the double peak is due to perfected spherulites. The melt–recrystallization model has been used to describe similar behavior in PLA and semicrystalline polymers in the literature [53,54]. Small imperfect crystalline spherulites realign and become more stable perfected spherulites, which creates an exothermic peak that divides the melting curve into two [53,55]. This process is dependent on heating rate, as recrystallization is a slow process. The shoulder behavior seen in our second heating curve agrees with the behavior seen at 10 °C as outlined by Yasuniwa et al. [53].

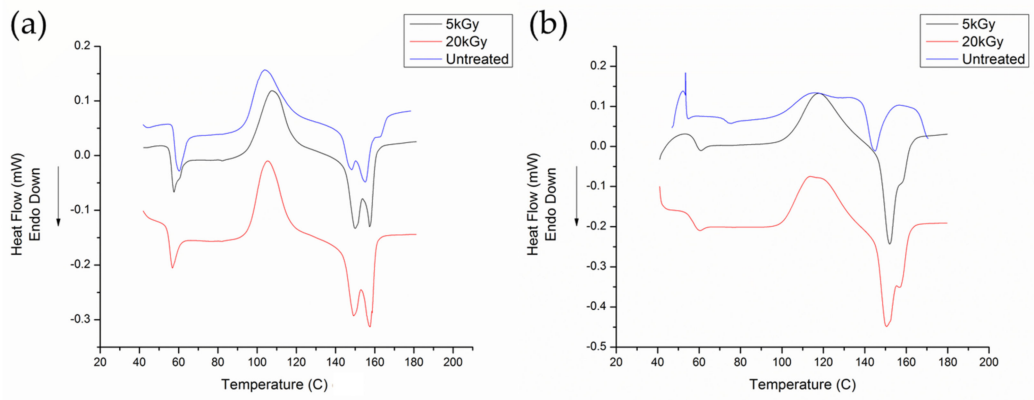

Figure 7. (**a**) Average cycle 1; (**b**) average cycle 2 for the unirradiated, 5 kGy, and 20 kGy samples.

3.4. Characterization with Optical Microscopy

To investigate the composition of the PLA samples, optical microscopy was used. Microscopy showed no optical activity when viewed with and without the polarized light. This indicates that the polymer is a racemic mixture of PDLA and PLLA because optical activity would be expected at other compositions. Optically active materials exhibit this property because they can rotate the plane of polarization due to differing amounts of enantiomers and their chirality; racemic mixtures of enantiomers are optically inactive because the equal and opposite rotations cancel out [28,56]. There were no changes in optical properties of irradiated samples.

3.5. XRD Analysis of Polymer Matrix Structure and Crystallinity

The diffractograms from both an unirradiated PLA sample and a 20 kGy irradiated PLA sample are shown in Figure 8. Both diffractograms demonstrate two wide peaks or halos: one from about 10° to 28° and the other from about 28° to 40°. Previous literature on the X-ray diffraction of highly amorphous PLA demonstrated that wide halos, such as the two observed in both samples measured, arise from diffraction patterns caused by the amorphous phase [57,58]. No sharp peaks corresponding to the presence of crystalline phase are observed, meaning that the PLA films, both before and after irradiation, are highly amorphous. However, there is a slight increase in the peak intensity of an initial wide amorphous halo from 10° to 28°. Previous X-ray diffraction studies of PLA indicate that an increase in peak intensity of this amorphous peak can be attributed to increases in crystallinity of the sample [59]. However, because this difference in peak intensity between samples is only on the order of 5%, more detailed characterization is necessary to ascertain more details about the crystallinity of the PLA.

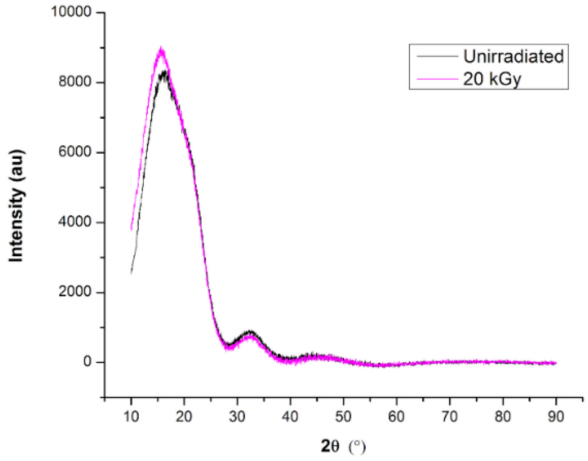

Figure 8. Diffractograms for unirradiated and 20 kGy irradiated PLA.

3.6. GPC Results

As shown by the molar mass distributions in Figure 9, there is no indication of an increase in molar mass with dose; thus, scission reactions are predominant under these conditions. Additionally, in Figure 10, we observed a loosely linear relationship between increasing dose (0–20 kGy) and a corresponding increase in the dispersity and decrease in M_n of the PLA films.

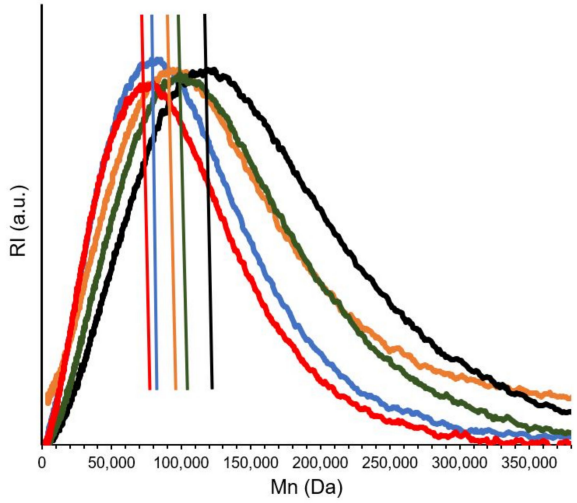

Figure 9. Number average molar mass distributions for the unirradiated sample (black) and samples irradiated at doses of 5 kGy (green), 10 kGy (orange), 15 kGy (blue), and 20 kGy (red). The lines represent the number average molar mass M_n value (center) of each trace at the peak of the distribution.

3.7. WVTR Calculation Results

For the WVTR analysis, three samples of each dose were weighed for six days. The WVTR was calculated using Equation (4), averaged, and plotted with the standard deviation shown in Figure 11. No significant trend was observed, as the standard deviation indicates high variability in the data. The thickness of the sample is higher than that of samples more commonly found in the literature while still meeting the requirements for the ASTM procedure [60–62].

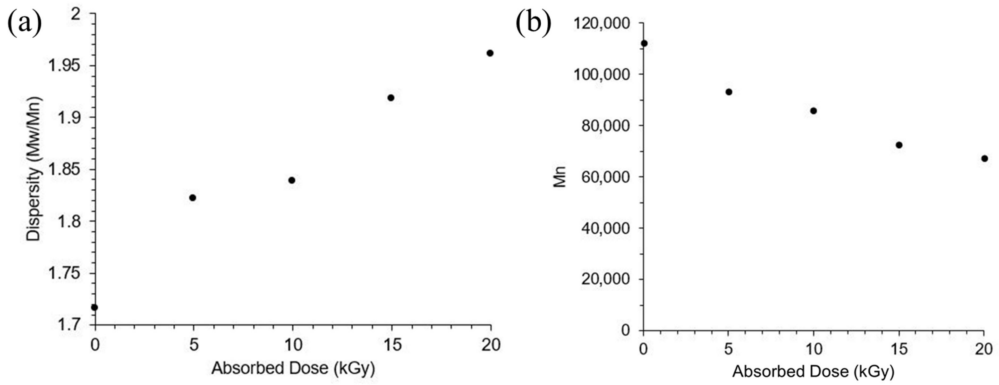

Figure 10. (**a**) Polymer dispersity as a function of absorbed dose of 0, 5, 10, 15, and 20 kGy, where dispersity is the weight average over number average molar mass; (**b**) number average molar mass M_n versus absorbed dose of 0, 5, 10, 15, and 20 kGy.

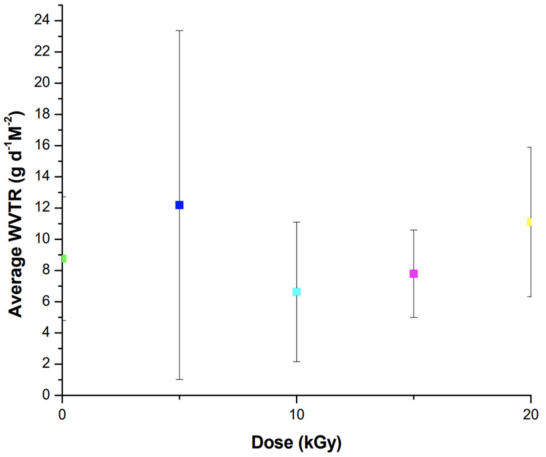

Figure 11. Water vapor transmission rate of PLA at 5 different doses: 0 kGy (light green), 5 kGy (dark blue), 10 kGy (light blue), 15 kGy (pink), 20 kGy (yellow). Each point represents the average of samples measured at each dose.

Analysis of the data indicates that there is no notable effect of irradiation dosage on WVTR of PLA. Based on the EPR and GPC results, an increase in the WVTR was expected after irradiation of the PLA. It has been shown that chain scission increases the WVTR of the polymer as it reduces the pathway tortuosity, or the number of barriers that the water vapor molecules must overcome [63,64]. However, in this study PLA was irradiated only up to a dose of 20 kGy and this resulted in low chain scission yields which did not have an impact in the WVTR.

4. Conclusions

Despite the fact that electron beam radiation provides a high dose rate and the absence of oxygen, the EPR and GPC results demonstrate that the predominant effect of radiation is the scission. The EPR results clearly show the formation of alkoxyl and C-centered radicals upon irradiation. The GPC data confirm the EPR results that the predominant effect of radiation is the scission. Upon irradiation with 20 kGy, M_n and M_w of the unirradiated samples decreased from 126,200 Da and 201,400 Da to 74,200 Da and 141,000 Da, respectively. The abstraction of H-atoms by alkoxyl radicals from neighboring molecules can also contribute to the formation of C-centered radicals. The GPC results also reveal the absence of higher-molecular-weight chains, which directly demonstrate the absence of crosslinking reactions of these C-centered radicals. This can be explained by the fact that these C-centered radicals react with the oxygen very rapidly since the irradiated samples

were exposed to air after irradiation. Due to the relatively low dose (maximum 20 kGy) and, consequently, the small induced scission yields, we have found that there is no change in T_g, only negligible (minor) changes in crystallinity, and no effect on water vapor transmission rate. Gel fraction measurements to measure crosslinking density were unsuccessful, as the gel point could not be reached. The absence of the formation of the three-dimensional gels supports the GPC findings. The presence of oxygen after irradiation can also contribute to the prevention of gel formation, since the reaction of C-centered radicals with oxygen compete to produce the corresponding peroxyl radicals. Finally, the change in oxidation index is very low, which is a good indicator that the irradiated PLA within this range of doses undergoes minimal degradation.

The main objective of this study is to evaluate the viability of PLA as a biodegradable food packaging material. Our results show that the irradiation has no effect on the aforementioned physical properties of the PLA. Therefore, this small degradation will enhance the biodegradability of this polymer for food irradiation and sterilization applications.

Author Contributions: Conceptualization, E.C.G.; methodology, J.C.H., O.L.M. and C.W.S.; formal analysis, C.A.L., J.R.B., E.C.G., J.C.H., K.L., C.W.S., A.C.F. and L.R.S.; investigation, J.R.B., E.C.G., A.H., K.L., C.W.S., C.A.L, R.L.B., A.C.F. and C.M.W.; data curation, E.C.G., O.L.M., K.L., C.A.L. and C.A.; writing—original draft preparation, E.C.G., J.C.H., K.L., O.L.M., C.W.S., S.M.W. and A.C.F.; writing—review and editing, E.C.G., K.G., J.C.H., K.L., O.L.M., C.W.S., A.U., A.C.F., C.M.W. and L.R.S.; visualization, C.A.L.; supervision, M.A.-S. and L.G.L.; project administration, E.C.G. and O.L.M.; funding acquisition, L.D. All authors have read and agreed to the published version of the manuscript.

Funding: This research was funded by the Maryland Sea Grant, National Oceanic and Atmospheric Administration, U.S. Department of Commerce under awards NA14OAR4170090 and NA18OAR4170070.

Institutional Review Board Statement: Not applicable.

Informed Consent Statement: Not applicable.

Data Availability Statement: Data are available from the authors upon reasonable request.

Acknowledgments: Kim Morehouse, Fred Bateman, the Gemstone Program at the University of Maryland, Kyle Ludwig, Jacques De Beer, Stas Stoliarov, and You Zhou.

Conflicts of Interest: The authors declare no conflict of interest. The funders had no role in the design of the study; in the collection, analyses, or interpretation of data; in the writing of the manuscript, or in the decision to publish the results. The statements, findings, conclusions, and recommendations are those of the authors and do not necessarily reflect the view of Maryland Sea Grant, the National Oceanic and Atmospheric Administration, or U.S. Department of Commerce.

References

1. Food and Agriculture Organization of the United Nations. *Food Wastage Footprint: Impacts on Natural Resources*; Food Wastage Footprint Summary—United Nations: Rome, Italy, 2013.
2. Gustavsson, J.; Cederberg, C.; Sonesson, U.; van Otterdijk, R.; Meybeck, A. *Global Food Losses and Food Waste: Extent, Causes and Prevention*; Swedish Institute for Food and Biotechnology, Food and Agriculture Organization of the United States: Rome, Italy, 2011; p. 37.
3. Holt-Giménez, E.; Shattuck, A.; Altieri, M.; Herren, H.; Gliessman, S. We already grow enough food for 10 billion people . . . and still can't end hunger. *J. Sustain. Agric.* **2012**, *36*, 595–598. [CrossRef]
4. Buzby, J.C.; Bentley, J.T.; Padera, B.; Campuzano, J.; Ammon, C. *Updated Supermarket Shrink Estimates for Fresh Foods and Their Implications for ERS Loss-Adjusted Food Availability Data*; Economic Information Bulletin; Economic Research Service of the U.S. Department of Agriculture: Washington, DC, USA, 2016.
5. United States Environmental Protection Agency. Facts and figures. In *Municipal Solid Waste Generation, Recycling, and Disposal in the United States: Facts and Figures for 2009*; Environmental Protection Agency: Washington, DC, USA, 2010; p. 13.
6. Puccini, S. The plastics problem part 1: Plastic packaging and the solid waste crisis. *Environs* **1992**, *16*, 21–34.
7. Geyer, R.; Jambeck, J.R.; Law, K.L. Production, use, and fate of all plastics ever made. *Sci. Adv.* **2017**, *3*, e1700782. [CrossRef]
8. Yang, L.; Paulson, A.T. Effects of lipids on mechanical and moisture barrier properties of edible gellan film. *Food Res. Int.* **2000**, *33*, 571–578. [CrossRef]

9. Debeaufort, F.; Martin-Polo, M.; Voilley, A. Polarity homogeneity and structure affect water vapor permeability of model edible films. *J. Food Sci.* **1993**, *58*, 426–429. [CrossRef]
10. Belay, Z.A.; Caleb, O.J.; Opara, U.L. Influence of initial gas modification on physicochemical quality attributes and molecular changes in fresh and fresh-cut fruit during modified atmosphere packaging. *Food Packag. Shelf Life* **2019**, *21*, 100359. [CrossRef]
11. Tsafrakidou, P.; Sameli, N.; Bosnea, L.; Chorianopoulos, N.; Samelis, J. Assessment of the Spoilage Microbiota in Minced Free-Range Chicken Meat during Storage at 4 °C in Retail Modified Atmosphere Packages. *Food Microbiol.* **2021**, *99*, 103822. [CrossRef]
12. Gómez-Estaca, J.; López-de-Dicastillo, C.; Hernández-Muñoz, P.; Catalá, R.; Gavara, R. Advances in Antioxidant Active Food Packaging. *Trends Food Sci. Technol.* **2014**, *35*, 42–51. [CrossRef]
13. Teixeira, G.H.A.; Cunha Júnior, L.C.; Ferraudo, A.S.; Durigan, J.F. Quality of Guava (*Psidium guajava* L. Cv. Pedro Sato) Fruit Stored in Low-O_2 Controlled Atmospheres Is Negatively Affected by Increasing Levels of CO_2. *Postharvest Biol. Technol.* **2016**, *111*, 62–68. [CrossRef]
14. Singh, S.P.; Pal, R.K. Controlled Atmosphere Storage of Guava (*Psidium guajava* L.) Fruit. *Postharvest Biol. Technol.* **2008**, *47*, 296–306. [CrossRef]
15. Conn, R.E.; Kolstad, J.J.; Borzelleca, J.F.; Dixler, D.S.; Filer, L.J.; Ladu, B.N.; Pariza, M.W. Safety Assessment of Polylactide (PLA) for Use as a Food-Contact Polymer. *Food Chem. Toxicol.* **1995**, *33*, 273–283. [CrossRef]
16. Cheng, Y.; Deng, S.; Chen, P.; Ruan, R. Polylactic Acid (PLA) Synthesis and Modifications: A Review. *Front. Chem. China* **2009**, *4*, 259–264. [CrossRef]
17. Lassalle, V.L.; Ferreira, M.L. Lipase-Catalyzed Synthesis of Polylactic Acid: An Overview of the Experimental Aspects. *J. Chem. Technol. Biotechnol.* **2008**, *83*, 1493–1502. [CrossRef]
18. Albertsson, A.-C.; Edlund, U.; Stridsberg, K. Controlled Ring-Opening Polymerization of Lactones and Lactides. *Macromol. Symp.* **2000**, *157*, 39–46. [CrossRef]
19. Gao, Q.; Lan, P.; Shao, H.; Hu, X. Direct Synthesis with Melt Polycondensation and Microstructure Analysis of Poly(L-lactic acid-*co*-glycolic acid). *Polym. J.* **2002**, *34*, 786–793. [CrossRef]
20. Datta, R.; Tsai, S.-P.; Bonsignore, P.; Moon, S.-H.; Frank, J.R. Technological and Economic Potential of Poly(lactic acid) and Lactic Acid Derivatives. *FEMS Microbiol. Rev.* **1995**, *16*, 221–231. [CrossRef]
21. Fahim, I.S.; Chbib, H.; Mahmoud, H.M. The Synthesis, Production & Economic Feasibility of Manufacturing PLA from Agricultural Waste. *Sustain. Chem. Pharm.* **2019**, *12*, 100142. [CrossRef]
22. Meekum, U.; Khiansanoi, A. PLA and Two Components Silicon Rubber Blends Aiming for Frozen Foods Packaging Applications. *Results Phys.* **2018**, *8*, 79–88. [CrossRef]
23. Aznar, M.; Ubeda, S.; Dreolin, N.; Nerín, C. Determination of Non-Volatile Components of a Biodegradable Food Packaging Material Based on Polyester and Polylactic Acid (PLA) and Its Migration to Food Simulants. *J. Chromatogr. A* **2019**, *1583*, 1–8. [CrossRef]
24. Ingrao, C.; Tricase, C.; Cholewa-Wójcik, A.; Kawecka, A.; Rana, R.; Siracusa, V. Polylactic Acid Trays for Fresh-Food Packaging: A Carbon Footprint Assessment. *Sci. Total Environ.* **2015**, *537*, 385–398. [CrossRef]
25. Weber, C.J. *Biobased Packaging Materials for the Food Industry: Status and Perspectives: A European Concerted Action*; KVL Department of Dairy and Food Science: Frederiksberg, Denmark, 2000.
26. Chandra, R. Biodegradable Polymers. *Prog. Polym. Sci.* **1998**, *23*, 1273–1335. [CrossRef]
27. Ahmed, J.; Varshney, S.K. Polylactides—Chemistry, Properties and Green Packaging Technology: A Review. *Int. J. Food Prop.* **2011**, *14*, 37–58. [CrossRef]
28. Saeidlou, S.; Huneault, M.A.; Li, H.; Park, C.B. Poly(lactic Acid) Crystallization. *Prog. Polym. Sci.* **2012**, *37*, 1657–1677. [CrossRef]
29. Suganuma, K.; Asakura, T.; Oshimura, M.; Hirano, T.; Ute, K.; Cheng, H.N. NMR Analysis of Poly(Lactic Acid) via Statistical Models. *Polymers* **2019**, *11*, 725. [CrossRef]
30. Luo, F.; Fortenberry, A.; Ren, J.; Qiang, Z. Recent Progress in Enhancing Poly(Lactic Acid) Stereocomplex Formation for Material Property Improvement. *Front. Chem.* **2020**, *8*, 688. [CrossRef] [PubMed]
31. Morehouse, K.; Komolprasert, V. *Irradiation of Food and Packaging: Recent Developments*; American Chemical Society: Washington, DC, USA, 2004; Volume 875.
32. Sommers, C.H.; Fan, X. *Food Irradiation Research and Technology*; John Wiley & Sons: Hoboken, NJ, USA, 2008.
33. Loo, J.S.C.; Ooi, C.P.; Boey, F.Y.C. Degradation of poly(lactide-*co*-glycolide) (PLGA) and poly(L-lactide) (PLLA) by electron beam radiation. *Biomaterials* **2005**, *26*, 1359–1367. [CrossRef] [PubMed]
34. Huang, Y.; Gohs, U.; Müller, M.T.; Zschech, C.; Wiessner, S. Electron Beam Treatment of Polylactide at Elevated Temperature in Nitrogen Atmosphere. *Radiat. Phys. Chem.* **2019**, *159*, 166–173. [CrossRef]
35. Malinowski, R. Effect of High Energy β-Radiation and Addition of Triallyl Isocyanurate on the Selected Properties of Polylactide. *Nucl. Instrum. Methods Phys. Res. Sect. B Beam Interact. Mater. At.* **2016**, *377*, 59–66. [CrossRef]
36. Shin, B.Y.; Han, D.H.; Narayan, R. Rheological and Thermal Properties of the PLA Modified by Electron Beam Irradiation in the Presence of Functional Monomer. *J. Polym. Environ.* **2010**, *18*, 558–566. [CrossRef]
37. Adamus-Wlodarcyzk, A.; Wach, R.A.; Ulanski, P.; Rosiak, J.M.; Socka, M.; Tsinas, Z.; Al-Sheikhly, M. On the Mechanisms of the Effects of Ionizing Radiation on Diblock and Random Copolymers of Poly(Lactic Acid) and Poly(Trimethylene Carbonate). *Polymers* **2018**, *10*, 672. [CrossRef]

38. Ashfaq, A.; Clochard, M.-C.; Coqueret, X.; Dispenza, C.; Driscoll, M.S.; Ulański, P.; Al-Sheikhly, M. Polymerization Reactions and Modifications of Polymers by Ionizing Radiation. *Polymers* **2020**, *12*, 2877. [CrossRef]
39. Benyathiar, P.; Selke, S.E.; Harte, B.R.; Mishra, D.K. The Effect of Irradiation Sterilization on Poly(Lactic) Acid Films. *J. Polym. Environ.* **2021**, *29*, 460–471. [CrossRef]
40. Melski, K.; Kubera, H.; Głuszewski, W.; Zimek, Z. Effect of Ionizing Radiation on the Properties of PLA Packaging Materials. *Nukleonika* **2011**, *56*, 65–69.
41. Paragkumar, N.T.; Edith, D.; Six, J.-L. Surface Characteristics of PLA and PLGA Films. *Appl. Surf. Sci.* **2006**, *253*, 2758–2764. [CrossRef]
42. Migliaresi, C.; Cohn, D.; De Lollis, A.; Fambri, L. Dynamic Mechanical and Calorimetric Analysis of Compression-Molded PLLA of Different Molecular Weights: Effect of Thermal Treatments. *J. Appl. Polym. Sci.* **1991**, *43*, 83–95. [CrossRef]
43. C16 Committee. *Test Methods for Water Vapor Transmission of Materials*; ASTM International: West Conshohocken, PA, USA, 2005. [CrossRef]
44. Von Sonntag, C. (Ed.) *Free-Radical-Induced DNA Damage and Its Repair: A Chemical Perspective*; Springer: Berlin/Heidelberg, Germany, 2006; pp. 77–86. [CrossRef]
45. Oliveira, J.E.; Mattoso, L.H.C.; Orts, W.J.; Medeiros, E.S. Structural and Morphological Characterization of Micro and Nanofibers Produced by Electrospinning and Solution Blow Spinning: A Comparative Study. *Adv. Mater. Sci. Eng.* **2013**, *2013*, e409572. [CrossRef]
46. Enumo, A.; Gross, I.P.; Saatkamp, R.H.; Pires, A.T.N.; Parize, A.L. Evaluation of Mechanical, Thermal and Morphological Properties of PLA Films Plasticized with Maleic Acid and Its Propyl Ester Derivatives. *Polym. Test.* **2020**, *88*, 106552. [CrossRef]
47. Garlotta, D. A Literature Review of Poly(Lactic Acid). *J. Polym. Environ.* **2001**, *9*, 63–84. [CrossRef]
48. Torres-Huerta, A.; Del Angel, D.; Domínguez-Crespo, M.A.; Palma Ramírez, D.; Perales-Castro, M.; Flores-Vela, A. Morphological and Mechanical Properties Dependence of PLA Amount in PET Matrix Processed by Single-Screw Extrusion. *Polym.-Plast. Technol. Eng.* **2016**, *55*, 1132433. [CrossRef]
49. Braun, B.; Dorgan, J.R.; Dec, S.F. Infrared Spectroscopic Determination of Lactide Concentration in Polylactide: An Improved Methodology. *Macromolecules* **2006**, *39*, 9302–9310. [CrossRef]
50. Saeidlou, S.; Huneault, M.A.; Li, H.; Sammut, P.; Park, C.B. Evidence of a Dual Network/Spherulitic Crystalline Morphology in PLA Stereocomplexes. *Polymer* **2012**, *53*, 5816–5824. [CrossRef]
51. Shao, J.; Xu, L.; Pu, S.; Hou, H. The Crystallization Behavior of Poly(L-Lactide)/Poly(D-Lactide) Blends: Effect of Stirring Time during Solution Mixing. *Polym. Bull.* **2021**, *78*, 147–163. [CrossRef]
52. Tsuji, H. Poly(Lactic Acid) Stereocomplexes: A Decade of Progress. *Adv. Drug Deliv. Rev.* **2016**, *107*, 97–135. [CrossRef] [PubMed]
53. Yasuniwa, M.; Tsubakihara, S.; Sugimoto, Y.; Nakafuku, C. Thermal Analysis of the Double-Melting Behavior of Poly(L-Lactic Acid). *J. Polym. Sci. Part B Polym. Phys.* **2004**, *42*, 25–32. [CrossRef]
54. Yasuniwa, M.; Satou, T. Multiple Melting Behavior of Poly(Butylene Succinate). I. Thermal Analysis of Melt-Crystallized Samples. *J. Polym. Sci. Part B Polym. Phys.* **2002**, *40*, 2411–2420. [CrossRef]
55. Yasuniwa, M.; Tsubakihara, S.; Ohoshita, K.; Tokudome, S. X-Ray Studies on the Double Melting Behavior of Poly(Butylene Terephthalate). *J. Polym. Sci. Part B Polym. Phys.* **2001**, *39*, 2005–2015. [CrossRef]
56. *Optically Active Polymers*; Selegny, E. (Ed.) Springer: Dordrecht, The Netherlands, 1979. [CrossRef]
57. Wang, Y.; Zhang, H.; Li, M.; Cao, W.; Liu, C.; Shen, C. Orientation and Structural Development of Semicrystalline Poly(Lactic Acid) under Uniaxial Drawing Assessed by Infrared Spectroscopy and X-ray Diffraction. *Polym. Test.* **2015**, *41*, 163–171. [CrossRef]
58. Picard, E.; Espuche, E.; Fulchiron, R. Effect of an Organo-Modified Montmorillonite on PLA Crystallization and Gas Barrier Properties. *Appl. Clay Sci.* **2011**, *53*, 58–65. [CrossRef]
59. Aliotta, L.; Cinelli, P.; Coltelli, M.B.; Righetti, M.C.; Gazzano, M.; Lazzeri, A. Effect of Nucleating Agents on Crystallinity and Properties of Poly (Lactic Acid) (PLA). *Eur. Polym. J.* **2017**, *93*, 822–832. [CrossRef]
60. Bhatia, A.; Gupta, R.K.; Bhattacharya, S.N.; Choi, H.J. Analysis of gas permeability characteristics of poly(lactic acid)/poly(butylene succinate) nanocomposites. *J. Nanomater.* **2012**, *2012*, 249094. [CrossRef]
61. Halasz, K.; Hosakun, Y.; Csóka, L. Reducing water vapor permeability of poly(lactic acid) film and bottle through layer-by-layer deposition of green-processed cellulose nanocrystals and chitosan. *Int. J. Polym. Sci.* **2015**, *2015*, 954290. [CrossRef]
62. Karkhanis, S.S.; Stark, N.M.; Sabo, R.C.; Matuana, L.M. Water vapor and oxygen barrier properties of extrusion-blown poly(lactic acid)/cellulose nanocrystals nanocomposite films. *Compos. Part Appl. Sci. Manuf.* **2018**, *114*, 204–211. [CrossRef]
63. Shogren, R. Water vapor permeability of biodegradable polymers. *J. Environ. Polym. Degrad.* **1997**, *5*, 91–95. [CrossRef]
64. Kantoğlu, Ö.; Güven, O. Radiation induced crystallinity damage in poly(L-lactic acid). *Nucl. Instrum. Methods Phys. Res. Sect. B Beam Interact. Mater. At.* **2002**, *197*, 259–264. [CrossRef]

Bibliography

[1] Food and Agriculture Organization of the United Nations, “Food Wastage Footprint: Impacts on Natural Resources,” United Nations, Summary, 2013. [Online]. Available: http://www.fao.org/3/i3347e/i3347e.pdf

[2] K. D. Hall, J. Guo, M. Dore, and C. C. Chow, “The Progressive Increase of Food Waste in America and Its Environmental Impact,” *PLOS ONE*, vol. 4, no. 11, p. e7940, Nov. 2009, doi: 10.1371/journal.pone.0007940.

[3] S. T. Hammond *et al.*, “Food Spoilage, Storage, and Transport: Implications for a Sustainable Future,” *BioScience*, vol. 65, no. 8, pp. 758–768, Aug. 2015, doi: 10.1093/biosci/biv081.

[4] “USDA ERS - Food Loss.” https://www.ers.usda.gov/data-products/food-availability-per-capita-data-system/food-loss/ (accessed Jul. 11, 2019).

[5] S. N. Yadav, W. Peterson, and K. W. Easter, “Do farmers overuse nitrogen fertilizer to the detriment of the environment?,” *Environ. Resour. Econ.*, vol. 9, no. 3, pp. 323–340, Apr. 1997, doi: 10.1007/BF02441403.

[6] “THE 17 GOALS | Sustainable Development.” https://sdgs.un.org/goals (accessed Mar. 28, 2022).

[7] E. Holt-Giménez, A. Shattuck, M. Altieri, H. Herren, and S. Gliessman, “We Already Grow Enough Food for 10 Billion People … and Still Can’t End Hunger,” *J. Sustain. Agric. - J Sustain. AGR*, vol. 36, pp. 595–598, Jul. 2012, doi: 10.1080/10440046.2012.695331.

[8] M. Robertson, *Sustainability Principles and Practice*, 2nd ed. Routledge, 2017.

[9] “Delayed Ripening Technology | ISAAA.org.” https://www.isaaa.org/resources/publications/pocketk/12/default.asp (accessed Mar. 28, 2022).

[10] T. A. E. C. Foundation, “Exploring America’s Food Deserts,” *The Annie E. Casey Foundation*, Feb. 14, 2021. https://www.aecf.org/blog/exploring-americas-food-deserts (accessed Mar. 28, 2022).

[11] K. M. Bower, R. J. Thorpe, C. Rohde, and D. J. Gaskin, “The intersection of neighborhood racial segregation, poverty, and urbanicity and its impact on food store availability in the United States,” *Prev. Med.*, vol. 58, pp. 33–39, Jan. 2014, doi: 10.1016/j.ypmed.2013.10.010.

[12] H. Williams, F. Wikström, T. Otterbring, M. Löfgren, and A. Gustafsson, “Reasons for household food waste with special attention to packaging,” *J. Clean. Prod.*, vol. 24, pp. 141–148, Mar. 2012, doi: 10.1016/j.jclepro.2011.11.044.

[13] A. Valdés, A. C. Mellinas, M. Ramos, M. C. Garrigós, and A. Jiménez, “Natural additives and agricultural wastes in biopolymer formulations for food packaging,” *Front. Chem.*, vol. 2, 2014, doi: 10.3389/fchem.2014.00006.

[14] J.-W. Rhim and P. K. W. Ng, “Natural Biopolymer-Based Nanocomposite Films for Packaging Applications,” *Crit. Rev. Food Sci. Nutr.*, vol. 47, no. 4, pp. 411–433, Apr. 2007, doi: 10.1080/10408390600846366.

[15] J. Markarian, “Biopolymers present new market opportunities for additives in packaging,” *Plast. Addit. Compd.*, vol. 10, no. 3, pp. 22–25, May 2008, doi: 10.1016/S1464-391X(08)70091-6.

[16] E. Chhabra, “How Trader Joe’s Is Cutting Down On Plastic,” *Forbes*.

https://www.forbes.com/sites/eshachhabra/2019/07/30/how-trader-joes-is-cutting-down-on-plastic/ (accessed Dec. 09, 2019).
[17] "The link between food waste and packaging | Greenbiz." https://www.greenbiz.com/article/link-between-food-waste-and-packaging (accessed Mar. 28, 2022).
[18] "What is PLA | A Comprehensive Guide to Polylactic Acid." https://www.goodstartpackaging.com/guide-to-pla-polylactic-acid/ (accessed Mar. 28, 2022).
[19] A. Oz, Ö. Süfer, and Y. Çelebi Sezer, "Poly (Lactic Acid) Films in Food Packaging Systems," vol. 2, Oct. 2017, doi: 10.23880/FSNT-16000131.
[20] J. Gómez-Estaca, C. López-de-Dicastillo, P. Hernández-Muñoz, R. Catalá, and R. Gavara, "Advances in antioxidant active food packaging," *Trends Food Sci. Technol.*, vol. 35, no. 1, pp. 42–51, Jan. 2014, doi: 10.1016/j.tifs.2013.10.008.
[21] D. Manas *et al.*, "The Effect of Irradiation on Mechanical and Thermal Properties of Selected Types of Polymers," *Polym. Basel*, vol. 10, no. 2, p. 158, 2018, doi: http://dx.doi.org/10.3390/polym10020158.
[22] C. Pin and J. Baranyi, "Predictive models as means to quantify the interactions of spoilage organisms," *Int. J. Food Microbiol.*, vol. 41, no. 1, pp. 59–72, May 1998, doi: 10.1016/S0168-1605(98)00035-X.
[23] N. Church, "Developments in modified-atmosphere packaging and related technologies," *Trends Food Sci. Technol.*, vol. 5, no. 11, pp. 345–352, Nov. 1994, doi: 10.1016/0924-2244(94)90211-9.
[24] F. Pasquali, G. Manfreda, P. Olivi, P. Rocculi, F. Sirri, and A. Meluzzi, "Modified-atmosphere packaging of hen table eggs: Effects on pathogen and spoilage bacteria," *Poult. Sci.*, vol. 91, no. 12, pp. 3253–3259, Dec. 2012, doi: 10.3382/ps.2012-02655.
[25] "Effect of anthocyanins on lipid oxidation and microbial spoilage in value-added emulsions with bilberry seed oil, anthocyanins and cold set whey protein hydrogels - ScienceDirect." https://www-sciencedirect-com.proxy-um.researchport.umd.edu/science/article/pii/S0308814618310379 (accessed Apr. 03, 2022).
[26] "The inhibitory effect of natural microflora of food on growth of Listeria monocytogenes in enrichment broths - ScienceDirect." https://www-sciencedirect-com.proxy-um.researchport.umd.edu/science/article/pii/S0168160510006677?casa_token=K7Jd-GF9atcAAAAA:KkYqiR-7Ys0KhH_GLUnO0ClWVR36rPFl5dX3d4oRcOh22qJ8K-UzkHIYTTKL5TbyJP2aSsNN2Q (accessed Apr. 03, 2022).
[27] G. J. Banwart, "Food Spoilage," in *Basic Food Microbiology*, G. J. Banwart, Ed. Boston, MA: Springer US, 1989, pp. 393–431. doi: 10.1007/978-1-4684-6453-5_8.
[28] W. Urbain, *Food Irradiation*. Elsevier, 2012.
[29] "What to know about food irradiation. How it works and is it dangerous," *LifeGate*, Feb. 06, 2017. https://www.lifegate.com/food-irradiation (accessed Mar. 23, 2021).
[30] C. for F. S. and A. Nutrition, "Regulatory Report on Irradiation of Food Packaging Materials," *FDA*, Jan. 2022, Accessed: Mar. 28, 2022. [Online]. Available: https://www.fda.gov/food/ingredients-additives-gras-packaging-guidance-documents-regulatory-information/regulatory-report-irradiation-food-packaging-materials
[31] C. for F. S. and A. Nutrition, "Guidance for Industry: Preparation of Food Contact Substance Notifications (Administrative)," *U.S. Food and Drug Administration*, Oct. 18,

2021. https://www.fda.gov/regulatory-information/search-fda-guidance-documents/guidance-industry-preparation-food-contact-substance-notifications-administrative (accessed Mar. 28, 2022).

[32] C. for F. S. and A. Nutrition, "Guidance for Industry: Preparation of Food Contact Substance Notifications (Toxicology Recommendations)," *U.S. Food and Drug Administration*, Oct. 18, 2021. https://www.fda.gov/regulatory-information/search-fda-guidance-documents/guidance-industry-preparation-food-contact-substance-notifications-toxicology-recommendations (accessed Mar. 28, 2022).

[33] "Frequently Asked Questions on Food Contact Notifications | PackagingLaw.com." https://www.packaginglaw.com/special-focus/frequently-asked-questions-food-contact-notifications (accessed Mar. 28, 2022).

[34] C. for F. S. and A. Nutrition, "Guidance for Industry: Submitting Requests under 21 CFR 170.39 Threshold of Regulation for Substances Used in Food-Contact Articles," *U.S. Food and Drug Administration*, Sep. 20, 2021. https://www.fda.gov/regulatory-information/search-fda-guidance-documents/guidance-industry-submitting-requests-under-21-cfr-17039-threshold-regulation-substances-used-food (accessed Mar. 28, 2022).

[35] "The Impact of Covid-19 on Food Security and Nutrition," United Nations, Jun. 2020. [Online]. Available: https://www.tralac.org/documents/resources/covid-19/3813-the-impact-of-covid-19-on-food-security-and-nutrition-un-policy-brief-june-2020/file.html

[36] J. Parfitt, M. Barthel, and S. Macnaughton, "Food waste within food supply chains: quantification and potential for change to 2050," *Philos. Trans. R. Soc. B Biol. Sci.*, vol. 365, no. 1554, pp. 3065–3081, Sep. 2010, doi: 10.1098/rstb.2010.0126.

[37] "Curbing food waste: Packaging to help manage a global challenge." https://www.packagingstrategies.com/articles/87839-curbing-food-waste-packaging-to-help-manage-a-global-challenge (accessed Apr. 03, 2022).

[38] A. Szymonik, *Logistics and Supply Chain Management*. 2012.

[39] Travis Minor *et al.*, "Economic Drivers of Food Loss at the Farm and Pre-Retail Sectors: A Look at the Produce Supply Chain in the United States," United States Department of Agriculture, EIB-216, Jan. 2020.

[40] R. R. Gundala and A. Singh, "What motivates consumers to buy organic foods? Results of an empirical study in the United States," *PLOS ONE*, vol. 16, no. 9, p. e0257288, Sep. 2021, doi: 10.1371/journal.pone.0257288.

[41] Sajal Kohli, Bjorn Timelin, Victor Fabius, and Sofia Moulvad Veranen, "How Covid-19 is changing consumer -behavior now and forever," McKinsey & Company, 2020.

[42] S. Yildirim *et al.*, "Active Packaging Applications for Food," *Compr. Rev. Food Sci. Food Saf.*, vol. 17, no. 1, pp. 165–199, 2018, doi: 10.1111/1541-4337.12322.

[43] P. Hauschild, R. F. Vogel, and M. Hilgarth, "Influence of the packaging atmosphere and presence of co-contaminants on the growth of photobacteria on chicken meat," *Int. J. Food Microbiol.*, vol. 351, p. 109264, Aug. 2021, doi: 10.1016/j.ijfoodmicro.2021.109264.

[44] S. Zabala, J. Castán, and C. Martínez, "Development of a time–temperature indicator (TTI) label by rotary printing technologies," *Food Control*, vol. 50, pp. 57–64, Apr. 2015, doi: 10.1016/j.foodcont.2014.08.007.

[45] L. Atarés and A. Chiralt, “Essential oils as additives in biodegradable films and coatings for active food packaging,” *Trends Food Sci. Technol.*, vol. 48, pp. 51–62, Feb. 2016, doi: 10.1016/j.tifs.2015.12.001.
[46] G. Simmonds, A. T. Woods, and C. Spence, “‘Show me the goods’: Assessing the effectiveness of transparent packaging vs. product imagery on product evaluation,” *Food Qual. Prefer.*, vol. 63, pp. 18–27, Jan. 2018, doi: 10.1016/j.foodqual.2017.07.015.
[47] B. Piqueras-Fiszman and C. Spence, “The influence of the feel of product packaging on the perception of the oral-somatosensory texture of food,” *Food Qual. Prefer.*, vol. 26, no. 1, pp. 67–73, Oct. 2012, doi: 10.1016/j.foodqual.2012.04.002.
[48] M. R. de Moura, L. H. C. Mattoso, and V. Zucolotto, “Development of cellulose-based bactericidal nanocomposites containing silver nanoparticles and their use as active food packaging,” *J. Food Eng.*, vol. 109, no. 3, pp. 520–524, Apr. 2012, doi: 10.1016/j.jfoodeng.2011.10.030.
[49] A. Mousavi Khaneghah, S. M. B. Hashemi, and S. Limbo, “Antimicrobial agents and packaging systems in antimicrobial active food packaging: An overview of approaches and interactions,” *Food Bioprod. Process.*, vol. 111, pp. 1–19, Sep. 2018, doi: 10.1016/j.fbp.2018.05.001.
[50] S. Ebnesajjad, “Introduction to Plastics,” in *Chemical Resistance of Engineering Thermoplastics*, E. Baur, K. Ruhrberg, and W. Woishnis, Eds. William Andrew Publishing, 2016, pp. xiii–xxv. doi: 10.1016/B978-0-323-47357-6.00021-0.
[51] P. Veiga-Santos, L. T. Silva, C. O. de Souza, J. R. da Silva, E. C. C. Albuquerque, and J. I. Druzian, “Coffee-cocoa additives for bio-based antioxidant packaging,” *Food Packag. Shelf Life*, vol. 18, pp. 37–41, Dec. 2018, doi: 10.1016/j.fpsl.2018.08.005.
[52] F. Garavand, M. Rouhi, S. H. Razavi, I. Cacciotti, and R. Mohammadi, “Improving the integrity of natural biopolymer films used in food packaging by crosslinking approach: A review,” *Int. J. Biol. Macromol.*, vol. 104, pp. 687–707, Nov. 2017, doi: 10.1016/j.ijbiomac.2017.06.093.
[53] M. L. Sanyang, S. M. Sapuan, M. Jawaid, M. R. Ishak, and J. Sahari, “Effect of plasticizer type and concentration on physical properties of biodegradable films based on sugar palm (arenga pinnata) starch for food packaging,” *J. Food Sci. Technol.*, vol. 53, no. 1, pp. 326–336, Jan. 2016, doi: 10.1007/s13197-015-2009-7.
[54] J.-W. Rhim, H.-M. Park, and C.-S. Ha, “Bio-nanocomposites for food packaging applications,” *Prog. Polym. Sci.*, vol. 38, no. 10–11, pp. 1629–1652, Oct. 2013, doi: 10.1016/j.progpolymsci.2013.05.008.
[55] G. Fuertes, I. Soto, R. Carrasco, M. Vargas, J. Sabattin, and C. Lagos, “Intelligent Packaging Systems: Sensors and Nanosensors to Monitor Food Quality and Safety,” *Journal of Sensors*, 2016. https://www.hindawi.com/journals/js/2016/4046061/ (accessed May 09, 2019).
[56] C. Vilela *et al.*, “A concise guide to active agents for active food packaging,” *Trends Food Sci. Technol.*, no. 80, pp. 212–222, doi: 10.1016/j.tifs.2018.08.006.
[57] P. Cazón, G. Velazquez, J. A. Ramírez, and M. Vázquez, “Polysaccharide-based films and coatings for food packaging: A review,” *Food Hydrocoll.*, vol. 68, pp. 136–148, Jul. 2017, doi: 10.1016/j.foodhyd.2016.09.009.
[58] R. Chandra, “Biodegradable polymers,” *Prog. Polym. Sci.*, vol. 23, no. 7, pp. 1273–1335, Nov. 1998, doi: 10.1016/S0079-6700(97)00039-7.
[59] Thian Eng San and Tan Yi Min, “Eco-friendly food packaging material doubles shelf-life of

food products," *ScienceDaily*, Accessed: May 09, 2019. [Online]. Available: https://www.sciencedaily.com/releases/2016/02/160223074732.htm
[60] Z. Shariatinia, "Pharmaceutical applications of chitosan," *Adv. Colloid Interface Sci.*, vol. 263, pp. 131–194, Jan. 2019, doi: 10.1016/j.cis.2018.11.008.
[61] Y. Cheng, S. Deng, P. Chen, and R. Ruan, "Polylactic acid (PLA) synthesis and modifications: a review," *Front. Chem. China*, vol. 4, no. 3, pp. 259–264, Sep. 2009, doi: 10.1007/s11458-009-0092-x.
[62] K. Goh *et al.*, "Sandwich-Architectured Poly(lactic acid)–Graphene Composite Food Packaging Films," *ACS Appl. Mater. Interfaces*, vol. 8, no. 15, pp. 9994–10004, Apr. 2016, doi: 10.1021/acsami.6b02498.
[63] S. Farah, D. G. Anderson, and R. Langer, "Physical and mechanical properties of PLA, and their functions in widespread applications — A comprehensive review," *Adv. Drug Deliv. Rev.*, vol. 107, pp. 367–392, Dec. 2016, doi: 10.1016/j.addr.2016.06.012.
[64] E. T. H. Vink, K. R. Rábago, D. A. Glassner, and P. R. Gruber, "Applications of life cycle assessment to NatureWorks™ polylactide (PLA) production," *Polym. Degrad. Stab.*, vol. 80, no. 3, pp. 403–419, Jan. 2003, doi: 10.1016/S0141-3910(02)00372-5.
[65] H.-M. Ng, S.-T. Bee, L. T. Sin, C. T. Ratnam, and A. R. Rahmat, "Effect of electron beam irradiation sterilization on biomedical polylactic acid composite filled with Scomberomorus Guttatus-derived hydroxyapatite," *Compos. Part B Eng.*, vol. 176, p. 107273, Nov. 2019, doi: 10.1016/j.compositesb.2019.107273.
[66] N. Mlalila, A. Hilonga, H. Swai, F. Devlieghere, and P. Ragaert, "Antimicrobial packaging based on starch, poly(3-hydroxybutyrate) and poly(lactic-co-glycolide) materials and application," *Trends Food Sci. Technol.*, no. 74, pp. 1–11.
[67] M. P. Arrieta, M. D. Samper, M. Aldas, and J. López, "On the Use of PLA-PHB Blends for Sustainable Food Packaging Applications," *Materials*, vol. 10, no. 9, Aug. 2017, doi: 10.3390/ma10091008.
[68] P. H. Yu, H. Chua, A. L. Huang, W. Lo, and G. Q. Chen, "Conversion of Food Industrial Wastes into Bioplastics," *ResearchGate*, Accessed: Oct. 29, 2019. [Online]. Available: https://www.researchgate.net/publication/5280368_Conversion_of_Food_Industrial_Wastes_into_Bioplastics
[69] S. Ebnesajjad, "Compostable Polymer Materials: Definitions, Structures,and Methods of Preparation," in *Handbook of Biopolymers and Biodegradable Plastics - Properties, Processing and Applications*, Elsevier, 2013, pp. 189–211.
[70] C. Jasso-Gastinel and J. Kenny, "Blends of PHB," in *Modification of Polymer Properties*, Elsevier, 2017, pp. 177–179.
[71] M. L. Tebaldi, A. L. C. Maia, F. Poletto, F. V. de Andrade, and D. C. F. Soares, "Poly(-3-hydroxybutyrate-co-3-hydroxyvalerate) (PHBV): Current advances in synthesis methodologies, antitumor applications and biocompatibility," *J. Drug Deliv. Sci. Technol.*, vol. 51, pp. 115–126, Jun. 2019, doi: 10.1016/j.jddst.2019.02.007.
[72] H.-J. Endres and A. Siebert-Raths, "Direct Biosynthesis of Biopolymers," in *Engineering Biopolymers - Markets, Manufacturing, Properties and Applications*, Hanser Publishers, 2011, pp. 105–106.
[73] F. Li, P. Biagioni, M. Bollani, A. Maccagnan, and L. Piergiovanni, "Multi-functional coating of cellulose nanocrystals for flexible packaging applications," *Cellulose*, vol. 20, no. 5, pp. 2491–2504, Oct. 2013, doi: 10.1007/s10570-013-0015-3.
[74] R. Chainey, "Which countries waste the most food?," *World Economic Forum*, 2015.

https://www.weforum.org/agenda/2015/08/which-countries-waste-the-most-food/ (accessed Oct. 07, 2019).
[75] Martin, "Sustainable consumption and production," *United Nations Sustainable Development*, 2016. https://www.un.org/sustainabledevelopment/sustainable-consumption-production/ (accessed Oct. 23, 2019).
[76] F. Hernández-Carmona, Y. Morales-Matos, H. Lambis-Miranda, and J. Pasqualino, "Starch extraction potential from plantain peel wastes," *J. Environ. Chem. Eng.*, vol. 5, no. 5, pp. 4980–4985, Oct. 2017, doi: 10.1016/j.jece.2017.09.034.
[77] K. dos Santos Caetano *et al.*, "Characterization of active biodegradable films based on cassava starch and natural compounds," *Food Packag. Shelf Life*, vol. 16, pp. 138–147, Jun. 2018, doi: 10.1016/j.fpsl.2018.03.006.
[78] W. N. Gilfillan, L. Moghaddam, J. Bartley, and W. O. S. Doherty, "Thermal extrusion of starch film with alcohol," *J. Food Eng.*, vol. 170, pp. 92–99, Feb. 2016, doi: 10.1016/j.jfoodeng.2015.09.023.
[79] G. Wypych, "10 - EFFECT OF PLASTICIZERS ON PROPERTIES OF PLASTICIZED MATERIALS," in *Handbook of Plasticizers (Third Edition)*, G. Wypych, Ed. ChemTec Publishing, 2017, pp. 209–332. doi: 10.1016/B978-1-895198-97-3.50012-3.
[80] M. Maiza, M. Benaniba, G. Quintard, and V. Massardier-Nageotte, "Biobased additive plasticizing Polylactic acid (PLA)," *Polímeros*, vol. 25, pp. 581–590, Dec. 2015, doi: 10.1590/0104-1428.1986.
[81] Y. Byun, Y. T. Kim, and S. Whiteside, "Characterization of an antioxidant polylactic acid (PLA) film prepared with α-tocopherol, BHT and polyethylene glycol using film cast extruder," *J. Food Eng.*, vol. 100, no. 2, pp. 239–244, Sep. 2010, doi: 10.1016/j.jfoodeng.2010.04.005.
[82] T. Mekonnen, P. Mussone, H. Khalil, and D. Bressler, "Progress in bio-based plastics and plasticizing modifications," *J. Mater. Chem. A*, vol. 1, no. 43, pp. 13379–13398, 2013, doi: 10.1039/C3TA12555F.
[83] Y. Liu, C. Pan, M. Ding, and J. Xu, "Effect of crosslinking distribution on gas permeability and permselectivity of crosslinked polyimides," *Eur. Polym. J.*, vol. 35, no. 9, pp. 1739–1741, Sep. 1999, doi: 10.1016/S0014-3057(98)00255-9.
[84] M. Kodal, A. A. Wis, and G. Ozkoc, "The mechanical, thermal and morphological properties of γ-irradiated PLA/TAIC and PLA/OvPOSS," *Radiat. Phys. Chem.*, vol. 153, pp. 214–225, Dec. 2018, doi: 10.1016/j.radphyschem.2018.10.018.
[85] R. Malinowski, "Effect of high energy β-radiation and addition of triallyl isocyanurate on the selected properties of polylactide," *Nucl. Instrum. Methods Phys. Res. Sect. B Beam Interact. Mater. At.*, vol. 377, pp. 59–66, Jun. 2016, doi: 10.1016/j.nimb.2016.04.028.
[86] R. Malinowski, "Mechanical properties of PLA/PCL blends crosslinked by electron beam and TAIC additive," *Chem. Phys. Lett.*, vol. 662, pp. 91–96, Oct. 2016, doi: 10.1016/j.cplett.2016.09.022.
[87] R. Dorati *et al.*, "gamma-irradiation of PEGd,lPLA and PEG-PLGA multiblock copolymers: II. effect of oxygen and EPR investigation," *AAPS PharmSciTech*, vol. 9, no. 4, pp. 1110–8, Dec. 2008, doi: 10.1208/s12249-008-9150-9.
[88] F. Urena-Nunez and S. Galindo, "Investigation of the electron paramagnetic resonance signal response in gamma-irradiated poly(lactic acid) for high-dose dosimetry," *Rev. Mex. Fis.*, vol. 64, no. 5, Jun. 2018.

[89] J. Zech *et al.*, “Noninvasive characterization (EPR, μCT, NMR) of 3D PLA electrospun fiber sponges for controlled drug delivery,” *Int. J. Pharm.*, Aug. 2020, doi: 10.1016/j.ijpx.2020.100055.
[90] P. Muller, “Glossary of terms used in physical organic chemistry (IUPAC Recommendations 1994),” *Pure Appl Chem*, vol. 66, no. 5, pp. 1077–1184, 1994, doi: 10.1351/pac199466051077.
[91] J. Weil and J. Bolton, *Electron Paramagnetic Resonance: Elementary Theory and Practical Applications*, 2nd ed. Hoboken, New Jersey: John Wiley & Sons, Inc., 2007.
[92] V. Chechik, E. Carter, and D. Murphy, *Electron Paramagnetic Resonance*. Oxford University Press, 2016.
[93] R. Drago, *Physical Methods for Chemists*. Saunders College Publishing, 1992.
[94] J. H. Gibbs and E. A. DiMarzio, “Nature of the Glass Transition and the Glassy State,” *J. Chem. Phys.*, vol. 28, no. 3, p. 373, Aug. 2004, doi: 10.1063/1.1744141.
[95] M. Abdelwahab, A. Flynn, B.-S. Chiou, S. Imam, W. Orts, and E. Chiellini, “Thermal, mechanical and morphological characterization of plasticized PLA-PHB blends,” *Polym. Degrad. Stab.*, vol. 97, no. 9, pp. 1822–1828, Sep. 2012, doi: 10.1016/j.polymdegradstab.2012.05.036.
[96] G. Ozkoc and S. Kemaloglu, “Morphology, biodegradability, mechanical, and thermal properties of nanocomposite films based on PLA and plasticized PLA,” *J. Appl. Polym. Sci.*, vol. 114, no. 4, pp. 2481–2487, Jul. 2009, doi: doi.org/10.1002/app.30772.
[97] K. W. Chew, T. C. Ng, and Z. H. How, “Conductivity and Microstructure Study of PLA-Based Polymer Electrolyte Salted with Lithium Perchloride, LiClO4,” *Int. J. Eletrochemical Sci.*, vol. 8, pp. 6354–6364, May 2013.
[98] C. Kittel, *Introduction to Solid State Physics*, 8th ed. Wiley, 2004.
[99] “How to Analyze Polymers Using X-ray Diffraction,” presented at the International Center for Diffraction Data, 2021. [Online]. Available: https://www.icdd.com/assets/tutorials/How-to-analyze-polymers.pdf
[100] S. B Aziz, A. S Marf, E. M. Dannoun, M. A. Brza, and R. M. Abdullah, “The Study of the Degree of Crystallinity, Electrical Equivalent Circuit, and Dielectric Properties of Polyvinyl Alcohol (Pva)-Based Biopolymer Electrolytes,” *Polymers*, vol. 12, no. 10, 2020, doi: 10.3390/polym12102184.
[101] A. Di Gianfrancesco, “8 - Technologies for chemical analyses, microstructural and inspection investigations,” in *Materials for Ultra-Supercritical and Advanced Ultra-Supercritical Power Plants*, A. Di Gianfrancesco, Ed. Woodhead Publishing, 2017, pp. 197–245. doi: 10.1016/B978-0-08-100552-1.00008-7.
[102] S. Saeidlou, M. A. Huneault, H. Li, and C. B. Park, “Poly(lactic acid) crystallization,” *Prog. Polym. Sci.*, vol. 37, no. 12, pp. 1657–1677, Dec. 2012, doi: 10.1016/j.progpolymsci.2012.07.005.
[103] “Mapping the Functional Tortuosity and Spatiotemporal Heterogeneity of Porous Polymer Membranes with Super-Resolution Nanoparticle Tracking | ACS Applied Materials & Interfaces.” https://pubs.acs.org/doi/full/10.1021/acsami.7b15335?casa_token=XMffPtn8PAsAAAAA%3ASho1PovM4DCnXV1PNQcvEUDWjSQgLqZTg23f1AxhZ-JRcUz8zzUCTu3vxCFEkXf3bJO9xJVrpR-Z62o& (accessed Mar. 28, 2022).
[104] “Introduction to Tensile Testing,” in *Tensile Testing*, 2nd ed., ASTM International. [Online]. Available:

https://www.asminternational.org/documents/10192/3465262/05105G_Chapter_1.pdf/e13396e8-a327-490a-a414-9bd1d2bc2bb8
[105] H. Lim and S. Hoag, "Plasticizer Effects on Physical–Mechanical Properties of Solvent Cast Soluplus® Films," *AAPS PharmSciTech*, vol. 14, May 2013, doi: 10.1208/s12249-013-9971-z.
[106] S. Farah, D. G. Anderson, and R. Langer, "Physical and mechanical properties of PLA, and their functions in widespread applications — A comprehensive review," *Adv. Drug Deliv. Rev.*, vol. 107, pp. 367–392, Dec. 2016, doi: 10.1016/j.addr.2016.06.012.
[107] K. Van de Velde and P. Kiekens, "Biopolymers: overview of several properties and consequences on their applications," *Polym. Test.*, vol. 21, no. 4, pp. 433–442, 2002, doi: 10.1016/S0142-9418(01)00107-6.
[108] T. J. Madera-Santana, R. Meléndrez, G. González-García, P. Quintana-Owen, and S. D. Pillai, "Effect of gamma irradiation on physicochemical properties of commercial poly(lactic acid) clamshell for food packaging," *Radiat. Phys. Chem.*, vol. 123, pp. 6–13, Jun. 2016, doi: 10.1016/j.radphyschem.2016.02.001.
[109] A. Enumo, I. P. Gross, R. H. Saatkamp, A. T. N. Pires, and A. L. Parize, "Evaluation of mechanical, thermal and morphological properties of PLA films plasticized with maleic acid and its propyl ester derivatives," *Polym. Test.*, vol. 88, p. 106552, Aug. 2020, doi: 10.1016/j.polymertesting.2020.106552.
[110] S. M. Razavi, S. Dadbin, and M. Frounchi, "Effect of gamma ray on poly(lactic acid)/poly(vinyl acetate-co-vinyl alcohol) blends as biodegradable food packaging films," *Radiat. Phys. Chem.*, vol. 96, pp. 12–18, Mar. 2014, doi: 10.1016/j.radphyschem.2013.08.010.
[111] C.-P. Wu, C.-C. Wang, and C.-Y. Chen, "Influence of asymmetric ratio of polystyrene-block-poly(methyl methacrylate) block copolymer on the crystallization rate of PLA," *Eur. Polym. J.*, vol. 66, pp. 160–169, May 2015, doi: 10.1016/j.eurpolymj.2015.02.018.
[112] L. Wang, X. Jing, H. Cheng, X. Hu, L. Yang, and Y. Huang, "Rheology and Crystallization of Long-Chain Branched Poly(L-lactide)s with Controlled Branch Length," *Ind. Eng. Chem. Res.*, vol. 51, pp. 10731–10741, Aug. 2012, doi: 10.1021/ie300524j.
[113] P. Nugroho, H. Mitomo, F. Yoshii, and T. Kume, "Degradation of poly(l-lactic acid) by γ-irradiation," *Polym. Degrad. Stab.*, vol. 72, no. 2, pp. 337–343, May 2001, doi: 10.1016/S0141-3910(01)00030-1.

Appendix A: Tensile Testing Methodology, Results, and Discussion

Methodology

Tensile testing was performed on unirradiated, 5kGy, 10 kGy, and 15 kGy dog-bone shaped samples with a cross-section of 0.30408 mm by 6.35 mm and a total gauge length of 12.7 mm (0.012"x 0.5"x 0.25") approximately six months after irradiation. A constant displacement rate of 2.5mm/min in tension was applied at room temperature using a Tinius Olsen H25K-T

benchtop universal testing machine. The resulting displacement force data was turned into engineering stress-strain graphs, which were then analyzed to determine ultimate tensile strength, elongation at break, Young's elastic modulus, and engineering yield strength at a 0.2% offset. These values were averaged for each dose rate and compared. Due to fragility of irradiated samples only two samples could be obtained per dose rate.

Results and Discussion

Average values of Young's modulus, ultimate tensile strength, the offset yield strength, and elongation at break were taken for each dose rate, with the exception of 20 kGy which was too fragile to obtain dog-bone shaped samples. The mechanical properties of the unirradiated films agree with what has been found in literature for PL(D,L)A [106], [107]. Young's modulus, ultimate tensile strength, yield strength, and elongation at break decreased slightly upon irradiation. Chain scission occurs in the dominant amorphous regions of our sample, decreasing the molecular weight throughout the bulk. This scission decreases the intermolecular forces between the chains, deteriorating the mechanical properties as the chains are more able to slide past one another without entanglement leading to weaker and less stiff samples that break at lower values of elongation [108]–[110]. The 15 kGy samples were observed to have higher mechanical properties than samples irradiated at lower dose rates. This could be due to radiation induced chain scission increasing crystallinity, requiring additional study of crystallinity using differential scanning crystallinity.

Table 1. Average values calculated using Stress-Strain curves obtained from tensile testing

Sample	Young's Modulus (MPa)	Ultimate Tensile Strength (MPa)	Offset Yield Strength (MPa)	50% Elongation at Break (%)
Unirradiated	2249 ± 45	57.13 ± 1.1	46.88 ± 0.94	6.240 ± 0.13
5 kGy	2192 ± 44	47.28 ± 0.95	42.73 ± 0.85	1.596 ± 0.032
10 kGy	1951 ± 39	44.00 ± 0.88	38.06 ± 0.76	1.856 ± 0.037
15 kGy	2171 ± 43	55.91 ± 1.1	44.84 ± 0.90	2.541 ± 0.051

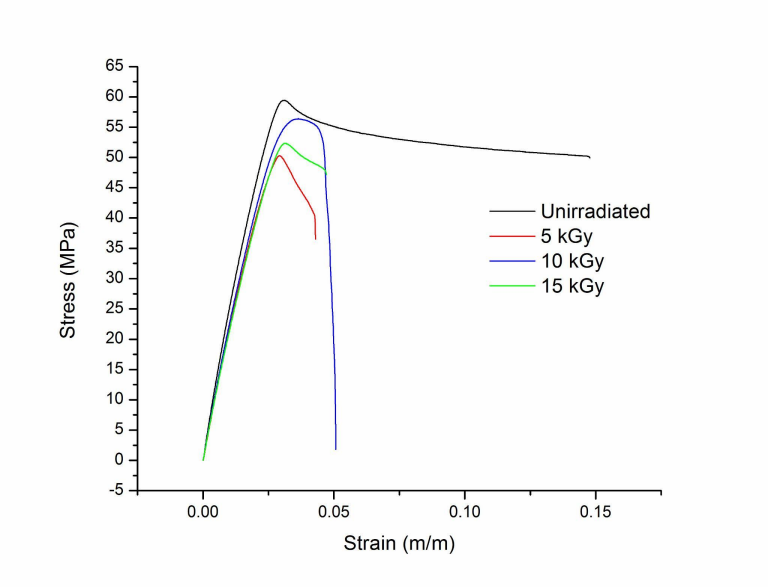

Figure 4. Representative stress-strain curves of unirradiated, 5 kGy, 10 kGy, and 15 kGy samples

Appendix B: Additional Differential Scanning Calorimetry Methodology, Results, and Discussion

Methodology

Further DSC analysis was performed on aged samples of about 5 mg in sealed aluminum pans in an oxygen atmosphere using a TA Instruments DSC 2500 approximately seven months after initial DSC analysis. The samples were subjected to the same two heating and cooling

cycles as previous experiments. In the first run, the samples equilibrated at 40 °C and then increased to 190 °C. They were held isothermal for five minutes at 190 °C before being cooled back down to 40 °C. The samples were again held isothermal for five minutes at 40 °C before increasing to 190 °C, where they were held isothermal for five minutes. Finally, the samples were cooled to 40 °C. For both heating cycles, the scanning rate was 10 °C min−1. From the resulting thermograms, attempts were made to measure the glass transition temperature (T_g), cold crystallization temperature (T_c), cold crystallization enthalpy (H_c), melting temperature (T_m), and melting enthalpy (H_m). Percent crystallinity ($\%X_c$) was calculated with the same methodology as previous experiments to determine if crystallization had developed in the irradiated samples.

Results and Discussion

Average values the glass transition temperature, the softening point, and the percent crystallinity were taken for aged 15 kGy and 20 kGy samples approximately seven months post-irradiation. Due to time limitations only two samples of each dose rate could be tested. 15 kGy samples were investigated due to their higher mechanical properties, with samples being obtained directly from remnants of the mechanical tests. The 20 kGy was obtained from 20 kGy samples that were too brittle to mechanically test in order to form a point of comparison between them and the 20 kGy samples utilized in DSC immediately after irradiation. No appreciable changes in crystallinity or transitions were observed after aging. Crystallinity was determined to be negligible for all samples. Steric hindrance of the side chains on the PLA backbone prevents crystallization and slows crystallization rates [111], [112]. This is likely what prevented further time-dependent recrystallization due to radiation-induced chain scission in the aged samples. Further study is needed to determine the higher mechanical properties of the 15 kGy samples as crystallinity is likely not the cause. Due to a very small sample size and the seven month aging

further study needs to be done. Furthermore, there is likely bias as only ductile samples could be tested with many 15 kGy samples being unable to be tested to the fragility and brittleness; a commonly accepted behavior in literature [108], [113].

Table 2. Average values of key thermal properties and crystallinity changes as a function of irradiation dose, calculated using DSC thermograms obtained from the first heating cycle.

Sample	Glass Transition (°C)	Softening Point (°C)	Percent Crystallinity (%)
Unirradiated	57.16 ± 1.1	150.1 ± 3.0	1.1 ± 0.02
Aged 15 kGy	55.1 ± 1.1	151.3 ± 3.0	0.76 ± 0.02
Initial 20 kGy	55.5 ± 1.1	151.9 ± 3.0	4.0 ± 0.08
Aged 20 kGy	55.2 ± 1.1	151.3 ± 3.0	2.1 ± 0.04

Table 3. Average values of key thermal properties and crystallinity changes as a function of irradiation dose, calculated using DSC thermograms obtained from the second heating cycle.

Sample	Glass Transition (°C)	Softening Point (°C)	Percent Crystallinity (%)
Unirradiated	60.8 ± 1.2	153.3 ± 3.1	1.2 (negligible)
Aged 15 kGy	58.3 ± 1.2	151.1 ± 3.0	2.5 ± 0.1
Initial 20 kGy	59.5 ± 1.2	151.2 ± 3.0	7.3 ± 0.2
Aged 20 kGy	58.7 ± 1.2	152.4 ± 3.0	1.6 ± 0.03

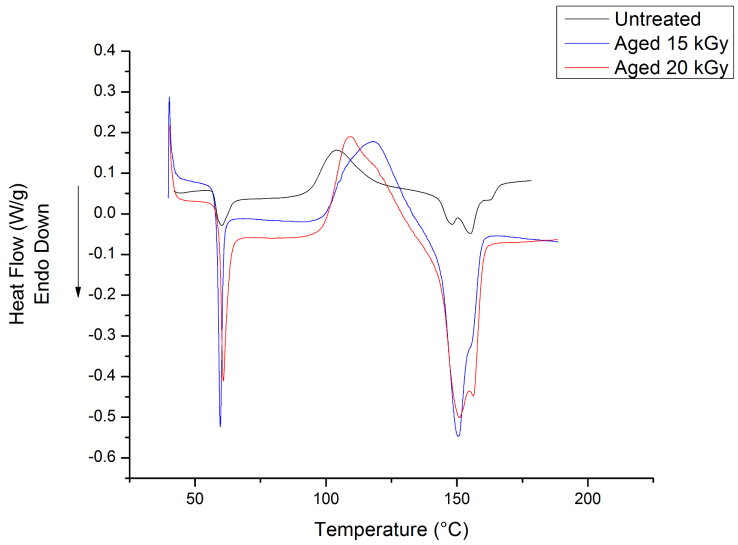

Figure 5. Average of the first heating cycle for Untreated, Aged 15 kGy, and Aged 20 kGy samples

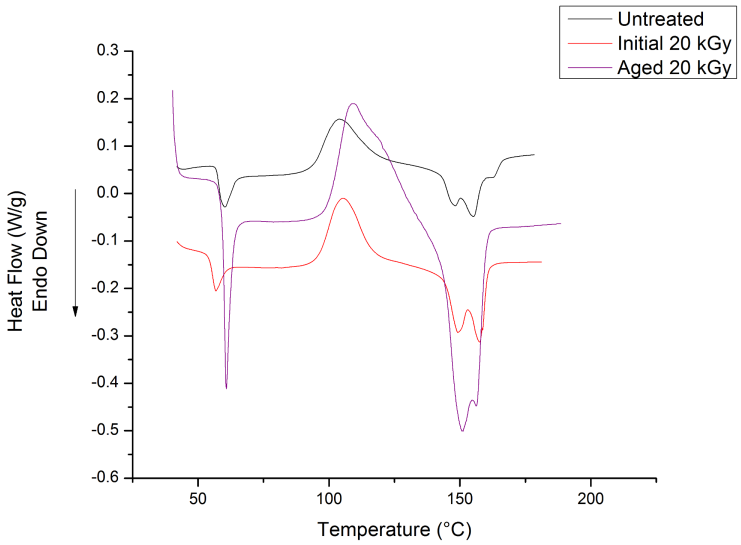

Figure 6. Average of the first heating cycle for Untreated, Initial 20 kGy, and Aged 20 kGy samples

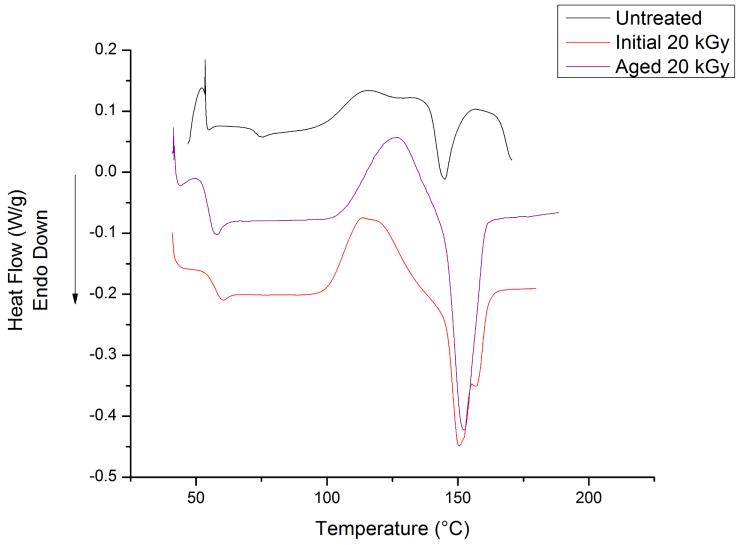

Figure 7. Average of the second heating cycle for Untreated, Initial 20 kGy, and Aged 20 kGy samples